FINDING ENERGY PATHWAYS FROM A TROPICAL ENERGY BUBBLE TO A MID-LATITUDE JET USING WAVE ACTIVITY FLUX VECTORS

by

Stephen A. Ogden

A thesis submitted in partial fulfillment of

the requirements for the degree of

Master of Science

(Atmospheric and Oceanic Sciences)

at the

UNIVERSITY OF WISCONSIN–MADISON

2014

Acknowledgments

I would like to thank my adviser, Professor Gregory Tripoli for the opportunity to work on this topic, along with encouragement and a few important pushes in the right direction. I'd also like to thank him for getting me up to speed on the topic so quickly, since this was something that had never been on my radar until after my first year of grad school.

I'd like to thank my parents for their support and encouragement over the years and for helping me to get to this point. Keeping things in perspective definitely helped me to get here, and they did a very good job of that.

Next, I'd like to thank Professor Matthew Hitchman for important insights at several points, none more important than directing me toward a paper that described wave activity flux—if I didn't see that paper, I might still be trying to make several dead-end strategies work to get these results. I'd also like to thank him and Professor Jonathon Martin for reading this thesis.

I'd like to thank my fellow students, especially the Tripoli and Martin groups, and especially the ones who repeatedly mentioned Eliassen-Palm fluxes before I recognized their utility. I definitely appreciated the help and conversation, even if I wasn't around 9 to 5 most days. I'd also like to thank Pete Pokrandt for technical assistance at various points.

Professor Gregory Tripoli and I also acknowledge Dr. Mel Shapiro, who proposed the idea that the amplification of the 6 November 2001 Rossby wave train

over the North Atlantic was a consequence of Hurricane Michelle.

Finally, I'd like to thank my various employers for financial support, including Professor Tripoli for letting me teach AOS 100/101.

Contents

List of Figures

Abstract

A large reservoir of of potential energy stored in the upper troposphere is a common feature to the tropics. This energy is supplied in large part by latent heating in tropical convection, some of which is tied to tropical cyclones. Pieces of this reservoir break off from the tropics intermittently, moving poleward and providing energy to the mid-latitude wave train. This energy manifests itself as enhanced jets (kinetic energy) and amplified troughs and ridges (potential energy). These features have a major effect on weather conditions at the surface.

Using Eliassen-Palm fluxes and energy conversion equations can help to track the quantity and quality of the energy transfer. Additionally, this energy can be tied to the overall meridional mass circulation, which can be tracked from the tropics to the mid-latitudes using isentropic coordinates. Using isentropic coordinates reveals the effect of baroclinic waves, which are both a requirement for and an effect of this energy transfer and conversion. An analysis of the connection between Hurricane Michelle and an amplified Rossby wave that has been shown to cause the catastrophic Algerian cyclone of November 2001 is used as an example of the effects of this energy transfer.

APPROVED

Advisor Title:

Professor Gregory Tripoli

University of Wisconsin-Madison

Department of Atmospheric and Oceanic Sciences

_____

Advisor Signature

_____

Date

Chapter 1: Introduction

The motivation of this paper is to connect the tropics to the extratropics using energy. There is no reason to believe that the extratropics are disconnected from the tropics, as is apparent when mid-latitude weather is affected by changes in the tropical atmosphere due to ENSO events. However, there is little well known about the underlying dynamics of these connections. This paper uses a case where a strong hurricane preceded an amplification of the mid-latitude wave train that led to an intense and damaging cyclone to document that connection.

The rest of this paper is divided as follows. A step by step layout of the pieces that compose the tropical-extratropical energy connection is done in Section 1. A case study of energy transfer based on Hurricane Michelle and a Mediterranean Sea cyclone in 2001 formatted for submission to an American Meteorological Society journal is given in Section 2. Potential future work and discussion are presented in Section 3.

1.1 The Basic Hadley Cell

Large-scale mass and energy circulations are important drivers of weather and climate across the globe, something that can easily be seen in the extratropics when those circulations are modified, such as during an El Nino or La Nina (Holton (2004); Straus and Shukla (2000); Rauber et al. (2012)). The best known of these circulations, the Hadley cell, is located from the Equator to around 30 degrees

latitude (also known as the subtropics). There are two Hadley cells, one on each hemisphere, though they do share the same upward branch near the Equator (Marshall and Plumb, 2008). The Hadley cell is the dominant component of meridional motion in the tropics. It brings air parcels upward along the Equator, horizontally poleward in the upper levels, downward at around 30 degrees latitude (or in the subtropics), and return them horizontally equatorward at low levels (Marshall and Plumb, 2008).

The forcing of this circulation is caused by what happens in each branch. The upward branch is associated with updrafts in convection rising from the warm surface, compounded by convective heating and mass addition along the Intertropical Convergence Zone (ITCZ) (Hartmann, 1994). Once this heating is completed, a lack of buoyancy in the far upper troposphere slows the rising (Stohl et al., 2003) and the poleward branch of the Hadley cell develops. The manifestation of the angular momentum these air parcels have leads to the creation of a jet as the air parcels move poleward and closer to the earth's axis of rotation (Marshall and Plumb, 2008). This effect turns the air parcels to the east, preventing further poleward motion and forcing the air parcels to move vertically as the restriction in poleward motion leads to convergence in the subtropics. Upward vertical motion is still impossible due to the statically stable stratosphere above, so any motion must be downward.

The sinking branch of the Hadley cell is commonly described as producing subtropical highs and deserts due to the drying that occurs in adiabatic descent

(Beer et al., 1977). The sinking is enhanced by radiative cooling, making air parcels cooler than the surrounding environment (Grotjahn, 2003). The return branch moving air parcels equatorward in the low levels then finishes the circuit due to convergence near the Equator created by convective updrafts in the rising branch (Gill, 1982). In the return branch, air parcels are heated by the warm ground or ocean and moistened by the ocean (Trenberth and Stepaniak, 2003), building up CAPE (assuming that the middle and upper tropospheric environment is not changing). The warm surface results from preferential heating of the tropics due to the surface's more direct angle to the sun's shortwave radiation (Petty, 2006). Additionally, there is a turning of the flow to the west, a phenomenon known as the trade winds (Hadley, 1735). This easterly motion adds angular momentum to air parcels in the return branch that will be lifted again in the rising branch of the Hadley cell (Marshall and Plumb, 2008).

However, the traditional isobaric Hadley cell just described is only a circulation in the tropics and is not explicitly linked to the rest of the atmosphere. The tropics are certainly not isolated from the extratropics (Trenberth and Stepaniak, 2003), requiring the connection to be caused by some method other than the isobaric Hadley cell. A true global energy balance requires input of shortwave energy from the sun to the tropics and output of infrared energy from the poles to space driven by differential heating due to the intensity of solar radiation at each location. This balance requires transport of energy across the entirety of each hemisphere (Marshall and Plumb, 2008), requiring a circulation that extends out of the tropics.

1.2 The Extended Hadley Cell

In pressure coordinates, this Hadley cell is the only large and persistent mass circulation seen in a zonally and time averaged meridional-height cross-section (Johnson, 1989). Looking at the averaged circulation, there appears to be no method to link the tropics with the extratropics. However, a transformation of the pressure coordinate vertical axis into potential temperature (or isentropic) coordinates, as done by Johnson, reveals a second portion of the Hadley cell circulation (Fig. 1.1, reproduced from Figure 8 of Johnson (1989)). This secondary portion extends the mass circulation of the Hadley cell well into the mid-latitudes by moving the sinking branch from the subtropics to the mid-latitudes and extending the horizontal branches to reach the new sinking branch. The rising branch along the Equator is not changed. Johnson describes this second portion as a geostrophic mode of mass transport, as opposed to the ageostrophic mode that describes the primary Hadley cell circulation pattern that only extends into the subtropics.

Johnson also points out that the secondary portion of the Hadley cell is defined by developing baroclinic waves creating transport of mass in the mid-latitudes. These baroclinic waves are a result of baroclinic instability due to differential heating between the warm tropics and colder extratropics. Once this instability begins to manifest itself, it appears as a wave structure (Gill, 1982). The structure can be seen as a displacement of the baroclinicity and attached air masses meridionally. By moving the baroclinicity meridionally, zonally alternating areas of poleward moving warm, tropical air and equatorward moving cold, polar air are

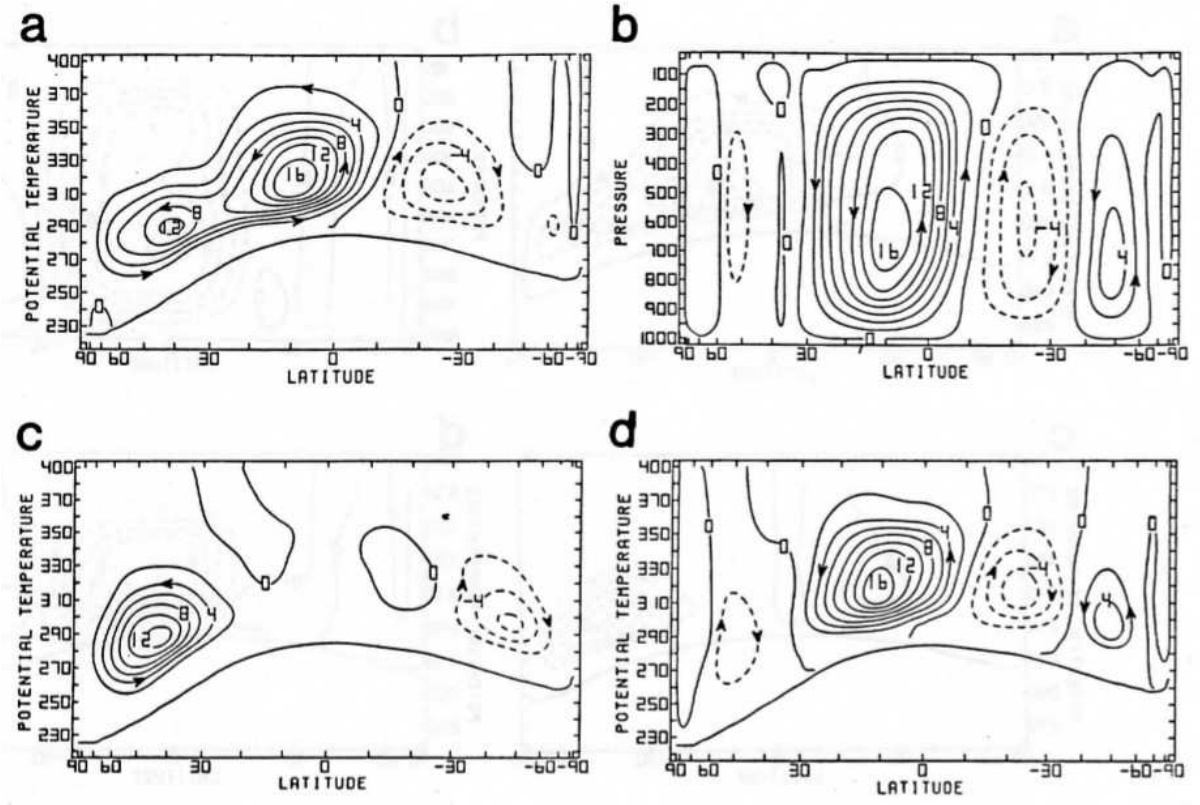

Figure 1.1: Zonally averaged mass streamfunctions (10^{10} kg/s) for January 1979, from Figure 8 of Johnson (1989). (a) Streamfunction in isentropic coordinates. (b) Streamfunction in isobaric coordinates. (c) Ageostrophic component of the isentropic coordinate circulation. (d) Geostrophic component of the isentropic coordinate circulation.

found in the low levels (Simmons and Hoskins, 1978). The same motion and air source structure can be found at greater height, though the particular temperatures change due to the lower height of the decreased static stability troposphere causing warmer air to be found in the extratropical stratosphere than the tropical stratosphere and upper troposphere (Marshall and Plumb, 2008). This meridional motion and temperature profile difference will also be important in energy transport, as will be discussed in later sections.

Another result of the development of baroclinic waves is the formation of a polar jet. Baroclinic waves form in the mid-latitudes, in areas where the Coriolis parameter is relatively high (Marshall and Plumb, 2008). There is a difference in the thickness of low level layers of varying temperature, with a given pressure surface over a cold surface having a lower height than over a warm surface due to it being thinner (Martin, 2006). Assuming near geostrophic conditions, this height and pressure gradient drives the creation of a wind, given by the thermal wind relation. The thermal wind relation,

$$\frac{du}{dz} = \frac{-R}{fp}\frac{dT}{dy}$$

(zonal component, where u is zonal wind, z is height, R is the universal gas constant, f is the Coriolis parameter, p is pressure, T is temperature, and y is meridional distance) describes an increase in the geostrophic wind with height perpendicularly over an area of strong low level temperature gradient (or baroclinicity). The geostrophic wind runs parallel to the baroclinic zone and is proportional to the magnitude of the baroclinicity. In the mid-latitudes, the wind is overall nearly geostrophic (Martin, 2006), meaning that a large change in the geostrophic wind causes a similar change in the actual observed wind. The area of strong winds over this baroclinicity is known as the polar jet (Shapiro and Keyser, 1990). The formation and structure of the polar jet and baroclinic waves will be a major component of poleward transport of energy, as discussed in a later section.

Individual baroclinic waves are not constant features, having a lifespan of a few days (Gill, 1982). This means that there is not a constant steady mass circulation from the tropics to the mid-latitudes, but rather that the mid-latitude portion of the circulation fluctuates in strength as the waves grow and decay, but the overall circulation appears to be one strength in a zonal and time average. The circulation could not be steady and constant due to the excessive kinetic energy needed to maintain the full circulation against frictional slowing, along with the fact that the mid-latitude circulation is unstable (Johnson, 1989).

1.3 The Mass-Energy Connection

The path of the global isentropic mass circulation is also the path of the global isentropic energy circulation, as the formulas for both are equivalent with the exception of multiplication by dry static energy (or Montgomery streamfunction (American Meteorological Society, 2014b)) in the energy circulation (Johnson (1989) equations 6.20 and 6.21). Adiabatic isentropic motion in the poleward horizontal branch allows for the tracking of dry static energy by mass transfer in that branch, assuming a constant dry static energy. A constant dry static energy is required in isentropic motion, as the change in the Montgomery streamfunction

$$M = C_p T + gz$$

is $$dM = C_p\, dT + g dz \quad ,$$

where C_p is the constant pressure heat capacity of air, T is temperature, g is the gravitational constant, and z is the height. The dry adiabatic lapse rate is defined as

$$\frac{dT}{dz} = \frac{-g}{C_p}$$

(American Meteorological Society, 2014a). As no heating or cooling occurs in isentropic motion due to its constant potential temperature, vertical motions must occur at the dry adiabatic lapse rate. Substituting the lapse rate into the temperature term in the change of Montgomery streamfunction gives

$$dM = C_p\,dT + gdz = C_p\left(\frac{-gdz}{C_p}\right) + gdz = -gdz + gdz = 0 \quad .$$

This ensures that mass and energy are linked in hydrostatic, isentropic motion. This rigid connection is not valid in the other branches, as dry static energy is gained in the equatorward branch due to heat fluxes off the surface (Grotjahn, 2003) and the upward branch due to latent heat release in moist convection (Grotjahn (2003); Fierro et al. (2009)), and lost in the sinking branch due to radiative cooling (Grotjahn (2003); Trenberth and Stepaniak (2003)). Nonetheless, the paths of each circulation are the same despite these dry static energy magnitude changes due to diabatic processes.

The connection between tropopause level and energy in the upper troposphere can be seen in the height of potential temperature surfaces and their thicknesses. A thick potential temperature layer leads to more volume and mass in a layer, assuming constant area. At the top of the layer is a cold anomaly as well, due to lifting the potential temperature surfaces above convection (Lang and Martin, 2013) at approximately the dry adiabatic lapse rate. Note that in the upper troposphere, the moist adiabatic lapse rate is nearly identical to the dry adiabatic

lapse rate (Hummel and Kuhn, 1981), so it matters little whether lifted air parcels are saturated (as in moist convection) in this situation. A cold anomaly is also a positive density anomaly compared to the areas around it at the same pressure, given constant pressure, due to the ideal gas law

$$p = \rho RT$$

decreases in temperature T must be countered by increases in density ρ, with p being pressure and R the universal gas constant. Since Montgomery streamfunction as defined is given in units of J/kg, a larger density gives more mass to contain the energy given a constant area. By having more mass (kg), a constant J/kg value leads to more Joules of energy. This can also be considered using the isentropic layer thickness, as a thicker isentropic layer gives larger volume to contain energy assuming constant area. The result is that there is more energy in the upper tropospheric/lower stratospheric layer that has a higher tropopause.

1.4 Tropical Cyclone Impact on Circulations

Tropical cyclones are an important part of the energy circulation. Large amounts of potential energy are produced in tropical cyclones from oceanic energy (Anthes and Johnson, 1968). Tropical cyclones also are able to move outside the isobaric Hadley cell (Hart, 2011), moving tropical air parcels into the mid-latitudes. This occurs due to the characteristic poleward turn tropical cyclones take, which leads any tropical cyclone that does not dissipate to exit the tropics and approach the mid-latitudes (Holland, 1983).

Tropical cyclone impacts on the mid-latitudes have been studied previously. Riemer et al. (2008) demonstrated the effects of an extratropical transitioning (ET) cyclone moving into an area with a straight jet, representing the westerlies in the mid-latitudes. In that analysis, the tropical cyclone forced a ridge that led to downstream baroclinic development (Orlanski and Sheldon, 1995). Riemer and Jones (2010) performed a more realistic simulation where an ET tropical cyclone approached a pre-existing wavy pattern, representing the mid-latitude Rossby wave train. That simulation provides a strikingly similar result to the case study of an actual event given in Section 2, where the ET tropical cyclone produces an amplified wave train.

There are multiple causes for this amplification. Riemer and Jones identified the tropical cyclone's upper level outflow as one cause, especially in the early stages of the interaction. Tropical cyclone outflow typically contains a characteristic upper level anticyclonic circulation and a local ridge in the pressure height and therefore potential temperature height fields (as latent heat release is occurring below) (Shi et al., 1990). When brought toward a mid-latitude wave train, the outflow creates or strengthens a ridge (Riemer and Jones, 2010). Downstream development theories state that this anticyclonic ridge development forces cyclonic troughs on either side of the ridge (Simmons and Hoskins, 1978). Riemer and Jones found this result experimentally, as troughs formed both upstream and downstream of the ET cyclone.

The development of jets due to ET cyclones were also investigated by Riemer and Jones. They found that the most important contributor to jet formation was upper level frontogenesis. The temperature gradient needed for this frontogenesis is directly relatable to the dry static energy, as higher heights of pressure and potential temperature surfaces associated with the tropical upper levels (which contain large amounts of dry static energy, partially due to latent heat release (Michaud and Derome, 1991) are also associated with colder temperatures compared to the warmer temperatures found at the same isentropic level in the extratropics (Marshall and Plumb, 2008). The counterintuitiveness of this combination of cold temperatures and large dry static energy is removed when the high heights and large geopotential energy in these areas are considered.

Additionally, zonal-eddy interaction plays a role in the effect of ET tropical cyclones on the mid-latitudes. Riemer and Jones (2010) and Grams et al. (2013) have both found that the position of the tropical cyclone is important to its effects on the mid-latitudes. Specifically, Grams et al. (2013) found the greatest growth of mid-latitude waves occurs when the tropical cyclone approaches the wave train just downstream of a trough (to the east in the westerlies, as occurred in the current case study) and the least growth occurs when the tropical cyclone approaches the wave train in the same location as a trough.

Given the persistent intense vertical motion present in tropical cyclone convection (Black et al., 1996) and tropical cyclones' tendency to acquire such convection in the tropics due to the much higher sea surface temperatures there

(Chimonas and Rossi, 1987) and the presence of hot towers in tropical cyclones (Fierro et al., 2009), it is possible to view tropical cyclones as a supercharging of the upward and poleward branches of the Hadley cell, whether the Hadley cell is viewed isentropically or isobarically. The interaction of the tropical cyclone-induced ridge and mid-latitude waves is also a factor in amplifying the waves, which will be discussed as zonal-eddy interaction throughout this paper.

1.5 The Tropical Energy Trap

Convection in the upward branch of the mass circulation produces large amounts of potential energy (Anthes and Johnson, 1968). Convection also places this mass and energy near its outflow level, in the tropical upper troposphere (Folkins et al., 2000). When this mass and energy becomes located in the upper levels of the tropical troposphere, it cannot move significantly away from its potential temperature surfaces there, creating a floor to trap the mass and energy. This is due to the combination of shortwave radiation from the sun being absorbed by ozone in the stratosphere and cloud-top cooling from convection below leading to no net temperature change at the bottom of the layer. This condition is known as being at the level of zero net radiative heating (Gettelman et al., 2004). Away from that level, divergence occurs due to diabatic heating (and rising) above and cooling (and sinking) below, reinforcing the trap and keeping mass in the trapped layer from moving significant vertical distances, which led Sherwood and Dessler (2003) to term this level the stagnation level.

An air parcel's inability to change its temperature without vertical motion at the level of zero net radiative heating causes it to retain the same potential temperature, forcing it to remain near the same potential temperature surface. As these potential temperature surfaces do not come near the surface in any area, they are in the upper part of what is known as the middleworld. Being in that location well above the surface (including in the tropics) also prevents any heating or cooling due to interaction with the boundary layer near the surface that can push these parcels off their potential temperature surface (Hoskins, 1991). However, the level of zero net radiative heating does not exist along those same isentropes in the extratropics; instead, the entire extratropical atmosphere is perpetually cooling to space due to lesser shortwave radiation absorption (Dopplick, 1972). If this mass and energy were simply able to move out to the extratropics, the air parcels containing it would cool and be able to move significant distances away from the potential temperature surfaces. However, there are two vertical walls to the trap that prevent this from occurring easily.

The other two walls of the trap are the subtropics. Large amounts of angular momentum are contained in tropical air parcels due to their location in the tropics, which is the area furthest away from the earth's axis of rotation. This angular momentum is augmented by the presence of easterly low level trade winds in the tropics that take momentum from the earth's rotation and increase angular momentum in low level parcels (Marshall and Plumb, 2008), which are then lifted by convection to create the energy referenced, seen as a time average throughout the

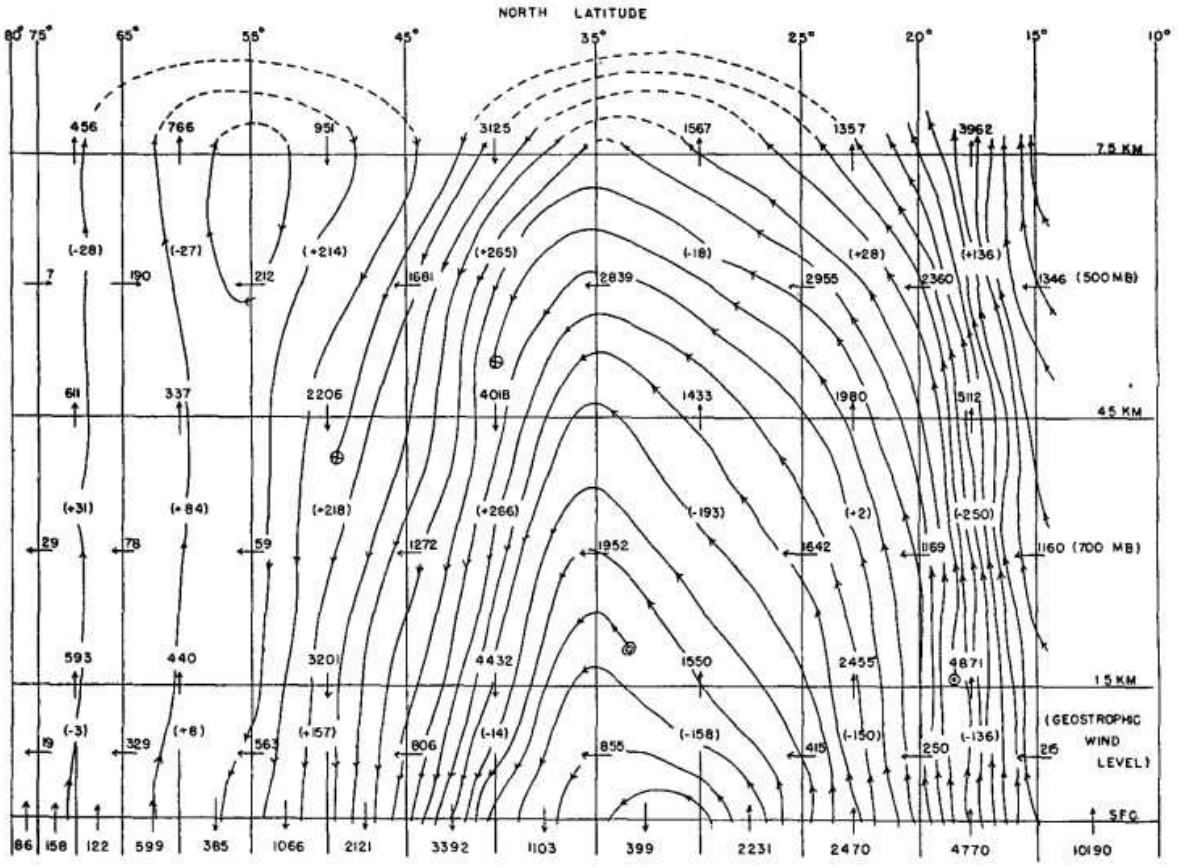

Figure 1.2: Net angular momentum generation (numbers along bottom) and transport (10^{29} g·cm^2/sec, arrows and attached numbers) for January 1946, from Figure 3 of Widger Jr (1949).

tropics in Figure 3 of Widger Jr (1949) (Fig. 1.2). The excess angular momentum does not manifest itself until the air parcels move poleward. As poleward motion occurs, the conserved angular momentum forces westerly winds, which turn motion eastward from the original poleward path. Mixing high angular momentum air parcels in the upper levels with high angular momentum air parcels in the low levels does nothing to reduce angular momentum and only reinforces the angular momentum walls of the trap. Should the poleward motion persist far enough, this westerly motion is expected to become unrealistically fast and well out of any balance. The

transition zone from realistic westerly winds to unrealistic (and unobserved) westerly winds occurs around 30 degrees latitude, in the subtropics (Marshall and Plumb, 2008). Based on the non-presence of unrealistic winds further poleward of the subtropics, the subtropics must comprise the other two walls of the trap for upper level energy in the tropics, observable as the subtropical jet. A look at a meridional cross-section shows that there is a lower tropopause height poleward of the subtropical jet (Fig. 1.3). This finding is corroborated by Shapiro and Keyser (1990) and their idealized cross-section of the tropopause level (their Figure 10.5). As described above, higher tropopause levels are an indicator of larger upper level dry static energy. Both cross-sections show areas of higher tropopause levels and therefore energy bounded on the poleward side by a jet.

If the boundaries of this trap were truly uncrossable, an infinite buildup of energy would be expected in the tropical upper levels, something that clearly does not happen. The potential temperature boundaries truly are uncrossable without some type of heating or cooling, as described above. Such heating or cooling is again impossible near the level of zero net radiative heating. In the extratropics, that level is not present in the upper troposphere or lower stratosphere where the potential temperature surfaces containing this energy are located (Fueglistaler et al., 2009). In order to get to the extratropics and cross the potential temperature boundaries, the subtropical angular momentum-caused boundary must be crossed. Therefore, there must be a method for crossing the subtropical boundaries that requires air parcels to retain their energy but lose their angular momentum.

1.6 Baroclinic Waves

Johnson describes a method of mixing out angular momentum vertically and zonally through kinetic energy development that would meet this demand. The method requires a developing baroclinic wave, just as the extended global circulation was described previously as needing baroclinic waves to exist. A developing baroclinic wave does not have a net transfer of mass, but it does have a net transfer of energy and momentum. The poleward portion of the wave preferentially moves a larger area of tropical air parcels in higher potential temperature levels that have large amounts of energy due to the greater height of the potential temperature surfaces they are on, while the equatorward portion of the wave preferentially moves a larger area of polar air parcels in lower potential temperature levels that have lesser amounts of energy due to their lower height (Johnson, 1989).

Development of a baroclinic wave in the mid-latitudes requires development of a jet along the wave due to the thermal wind balance becoming important in mid-latitude baroclinic (large temperature gradient) areas (Gill, 1982). This balance is a result of a height gradient in the upper levels, caused by the low level temperature gradient as described previously. However, it is not necessary for the pressure gradient to be fully forced from below–it can also be created in the upper levels by a temperature gradient created by upper level frontogenesis (Lang and Martin, 2012). The thermal wind describes a change in geostrophic wind with height. It is possible to describe the formation of a westerly jet by the existence of a

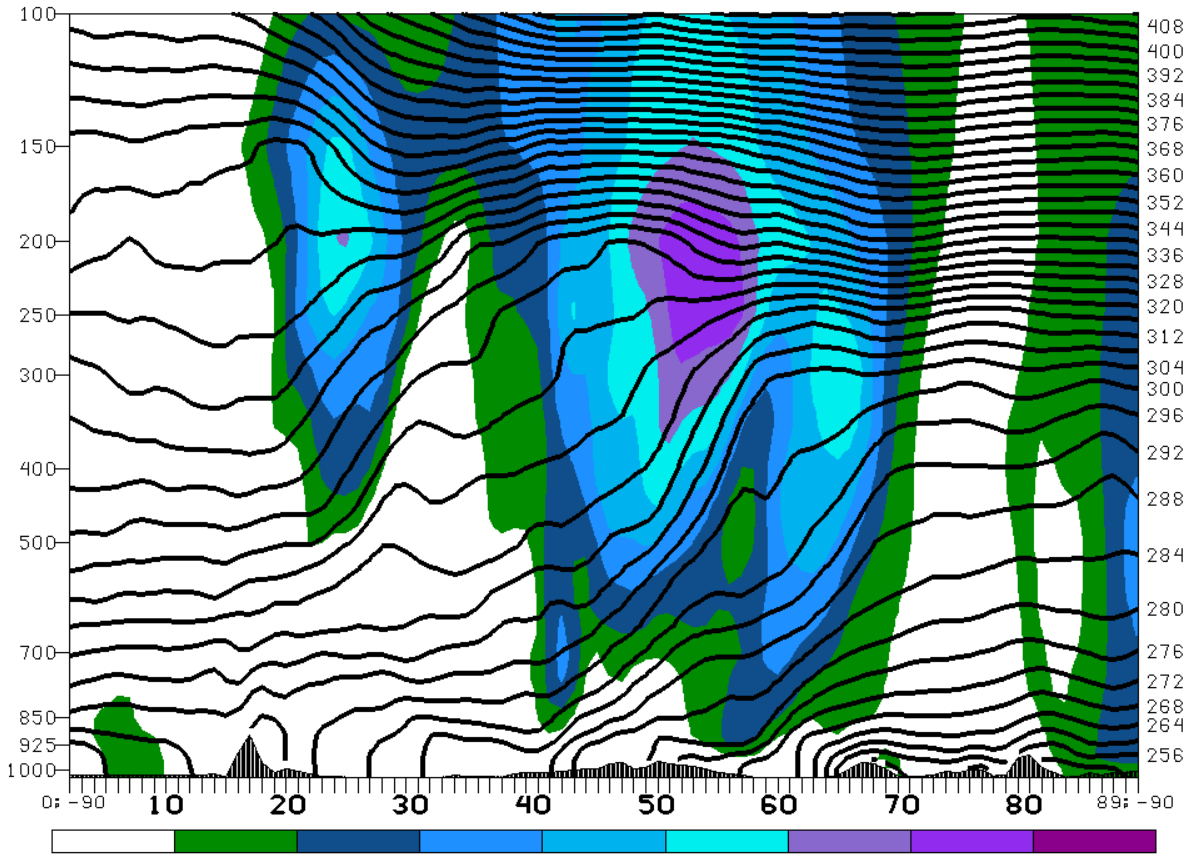

Figure 1.3: Meridional cross-section of zonal wind (fill) every 10 knots starting at 10 knots and potential temperature (contours) every 4 degrees Kelvin at 90 degrees West from the Equator to the North Pole at 18 UTC 30 Oct 2001. Vertical axis is pressure.

reversed (compared to the surface) temperature gradient above the jet. Cold air in the tropics and warm air in the extratropics creates an opposite sign of dT/dy compared to the surface. As the other components of the thermal wind relation do not change sign with height, the sign of du/dz changes to negative. This represents a decrease in wind with height, or an increase in wind with lowering height. Based on the presence of a jet near to below the mid-latitude tropopause and the existence of the reversed temperature gradient above the mid-latitude tropopause based on

upward displacement of potential temperature surfaces in the tropics (Marshall and Plumb, 2008), this reversed thermal wind relation is valid to at least partially describe the formation of a polar jet.

Developing a jet requires the production of eddy kinetic energy, as faster moving air is defined to have far greater amounts of kinetic energy than the same mass of slower moving air due to the dependence of kinetic energy on wind speed squared (Grotjahn, 2003). This jet is also an anomaly from the zonal mean, requiring it to contain large amounts of eddy kinetic energy instead of zonal mean kinetic energy. The source of this eddy kinetic energy must be some other form of energy, zonal mean kinetic, potential, internal and/or latent heat release. Both potential and internal energies are accounted for in dry static energy, potential represented by height and internal by temperature. Extra potential energy in the tropics is apparent in the height of potential temperature surfaces in the tropical upper troposphere as compared to the extratropics, which leads to reduced internal energy as the actual temperature is lower than in the extratropics along some potential temperature surfaces (Marshall and Plumb, 2008). The lack of moisture in the upper atmosphere and the small difference between the moist and dry adiabatic lapse rates (Hummel and Kuhn, 1981) precludes any warming or significant energy contribution from latent heat release. Therefore, it is expected that a portion of the energy used to produce eddy kinetic energy is potential energy. Zonal mean kinetic energy is also a candidate for producing eddy kinetic energy. Energy conversion from both of these energy sources will be investigated in Section 2.

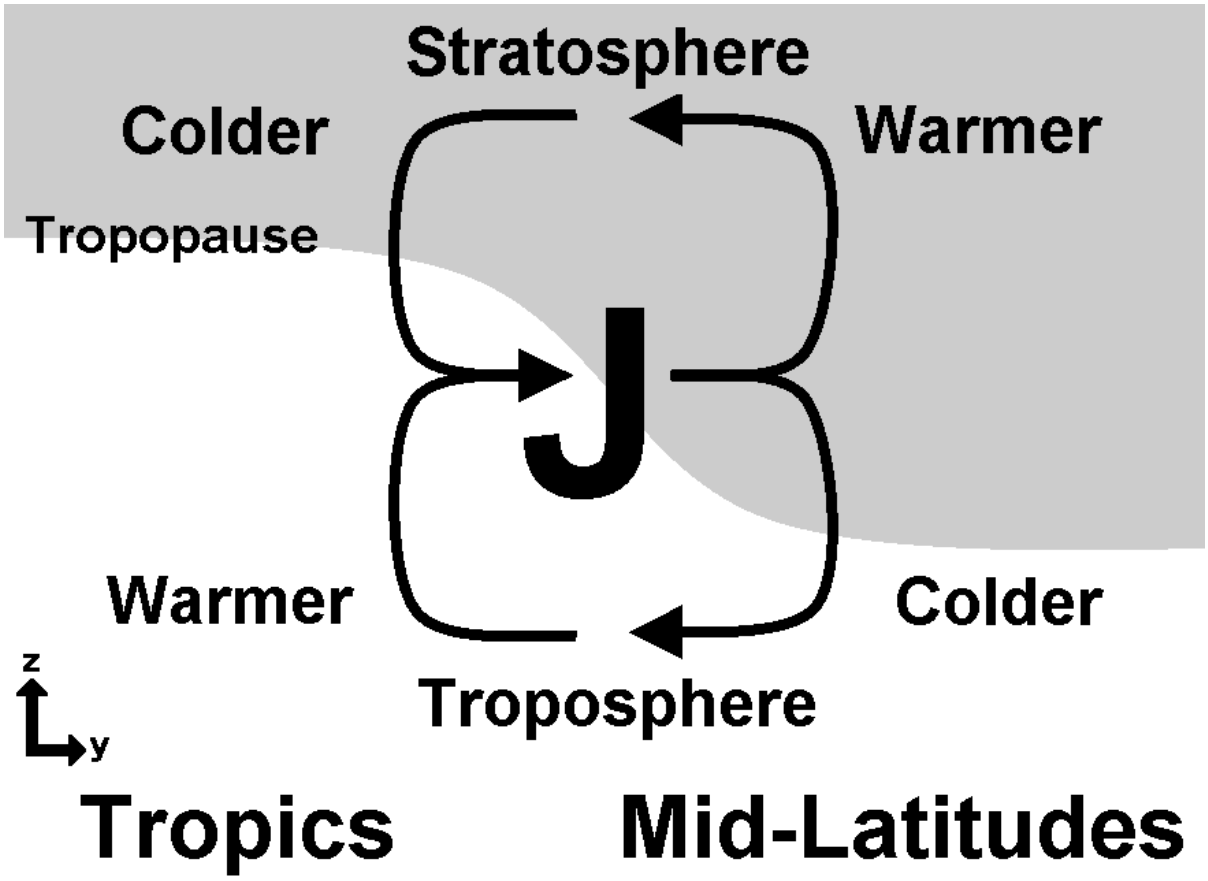

Figure 1.4: Diagram of jet entrance Sawyer-Eliassen circulations. Perspective is similar to Figure 1.3. White (gray) represents troposphere (stratosphere). "Warmer" and "colder" are relative to that height. X axis is latitude and Y axis is height. Adapted from Tripoli (2013).

1.7 Local Circulations

In the process of developing a jet, Sawyer-Eliassen circulations also form on each end of the jet. Assuming no temperature advection along the jet, the classic four cell model of Sawyer-Eliassen circulations features the entrance region circulation having rising air on the tropospheric equatorward (warm) side and sinking air on the tropospheric poleward (cold) side. The motion between these two areas

must be across the jet toward the pole (Martin, 2006) (Fig. 1.4). This is a thermally direct circulation, which would be expected to use potential energy (Namias and Clapp, 1949). The stratospheric vertical motions are reversed, with sinking motion on the equatorward (cold) side and rising motion on the poleward (warm) side (Lang and Martin, 2012). This upper circulation is in the extratropical stratosphere, but in the tropical upper troposphere as the tropopause is much higher in the tropics (Marshall and Plumb, 2008). Note that the pole-Equator temperature gradient is reversed in the stratosphere and tropical upper troposphere, maintaining the thermally direct nature of the vertical portions of the circulation. Note also that mass conservation requires the across-jet motion to again be poleward for the upper circulation, adding to the poleward motion in the lower circulation.

In the exit region, the circulations are reversed, giving a thermally indirect circulation that would be expected to recreate potential energy and an across-jet motion equatorward (Martin, 2014). The presence of geostrophic temperature advection by the jet only pushes the rising and sinking motions to remain with the temperature gradient. The thermally direct/indirect and across-jet patterns remain generally in place (Lang and Martin, 2012).

The strength of the motion in the Sawyer-Eliassen circulations depends on several factors. The most important in an analysis of energy conversion is static stability. Static stability affects the vertical motions in the circulations, as high static stability air resists vertical motion better than low static stability air (Burger, 1988). Increasing the strength of the equatorward vertical branch strengthens the

circulation due to mass continuity, which then forces more across-jet motion (Uccellini and Kocin, 1987). The strengthening of a jet (which requires a strengthening of the Sawyer-Eliassen circulation) by stronger vertical motion in lower static stability air has been investigated in the context of convection decreasing static stability in the equatorward side of the jet entrance region (Lang and Martin, 2013). However, there is no reason to believe that the effect would be any different if the lower static stability were brought in from another region. The result would still lead to the strengthening of both equatorward side vertical motions, which strengthens the entire circulation. These motions are another form of eddy kinetic energy produced from potential energy in the form of higher heights of potential temperature surfaces in the tropical upper levels (Holton, 2004). Once on the poleward side of the jet, stratification differences between the troposphere (lower) and stratosphere (higher) would lead to a preferential strengthening of the tropospheric poleward side downward vertical motion, as the statically stable extratropical stratosphere would resist vertical motion (Burger, 1988). These Sawyer-Eliassen circulations will play an important role in angular momentum movement, as explained in a later section.

Chapter 2: Michelle-Wave Case Study

2.1 Introduction

Global energy balance requires a gain of energy due to solar shortwave radiation preferentially heating the tropics to be balanced by a loss of energy due to atmospheric longwave radiation preferentially being emitted to space in the extratropics (Petty, 2006). Global atmospheric circulations are required to maintain this flow of energy, but the major well-known isobaric circulation (the Hadley cell) only accounts for a portion of the necessary movement, as it only extends from the tropics to the subtropics (Marshall and Plumb, 2008). Additional circulations must be present to bring this energy out of the subtropics. It is baroclinic waves that compose the additional circulations and provide the necessary conditions to move energy into the extratropics (Johnson, 1989). A case study of the effect of the extended circulation will be performed to connect energy in the tropics partially associated with Hurricane Michelle in 2001 to an amplified mid-latitude Rossby wave pattern several days later that led to an intense cyclone in the Mediterranean (Tripoli et al., 2005).

The remainder of this chapter will be organized as follows: in Section 2.2, a short description of the composition of the structures causing this transfer of energy. The role of the Sawyer-Eliassen circulation in this energy transfer will be discussed in Section 2.3. Section 2.4 is a description of the metrics used to describe the energy and its movement by these structures. Section 2.5 is a full day-by-day description of the case and the metrics occurring in it. Conclusions will be given in Section 2.6.

2.2 Background

The isobaric Hadley cell is the most commonly known global mass and energy circulation, but it only reaches from the Equator to around 30 degrees latitude (Marshall and Plumb, 2008). No notable circulation is present in the mid-latitudes in isobaric coordinates, appearing to prevent any meaningful exchange between the tropics and the extratropics. However, a transformation to isentropic coordinates produces an extension of the Hadley cell into the mid-latitudes (Johnson, 1989). This extension allows for mass and energy exchange between the tropics and extratropics, with upper level isentropic motion leaving the tropics and lower level isentropic motion entering the tropics. Johnson describes this extension as being caused by developing baroclinic waves.

Baroclinic waves away from the Equator lead to jet formation based on the thermal wind relation. The polar jet in the mid-latitudes is due to the thermal gradient between the cold polar atmosphere and the warm tropical atmosphere, creating a geopotential height gradient in the mid-latitude upper levels (Martin, 2006). This height gradient can also be forced in the upper levels by upper level temperature differences due to upper level frontogenesis (Lang and Martin, 2012), which occur in an opposite pattern as the lower levels—colder air sits toward the equator in the upper levels, instead of toward the poles as in the lower levels. If this occurs, the sign of du/dz in the thermal wind equation switches, making the wind decrease with height, or increase going down.

The upper level temperature gradient is created by a higher tropopause in the tropics that causes the troposphere to extend higher, leading to colder temperatures there (Marshall and Plumb, 2008). The colder temperatures are also the location of higher heights of potential temperature surfaces and excess potential energy, as potential energy is proportional to height. These potential temperature surfaces are the location of large amounts of dry static energy due to their large geopotential heights. This dry static energy would then be expected to follow the mass circulation (Johnson, 1989).

The poleward edge of the isobaric Hadley cell is a location where the mass circulation requires baroclinic waves to continue any poleward movement as the Hadley cell extends no further poleward (Johnson, 1989). Vertical motion is restricted by the potential temperature of the high energy air parcels, as any motion is required to be isentropic unless there is a heating or cooling. Such heating or cooling is precluded by the high energy air parcels' location in the tropical upper troposphere, where the level of zero net radiative heating is located (Gettelman et al., 2004). In this location, the cooling from convection below and heating from ozone absorbing shortwave energy above balance to prevent any temperature change. The two aforementioned forcings also lead to divergence away from this level, which is also known as the stagnation level due to the lack of significant vertical motion at that level (Sherwood and Dessler, 2003). Further poleward motion in the isobaric Hadley cell is restricted by conservation of angular momentum while moving toward the earth's axis of rotation, along with the imposition of additional

angular momentum by trade winds during the air parcel's movement in the lower levels of the Hadley cell, forcing eastward movement (Marshall and Plumb, 2008).

The role of baroclinic waves in this energy transport is to provide a method to remove the excess angular momentum from the high energy air parcels via pressure stresses (Johnson, 1989) as potential energy is converted to eddy kinetic. Mixing the upper level tropical high energy, high angular momentum with lower level mid-latitude lower energy, lower angular momentum air removes angular momentum from the poleward moving tropical air and places it in the equatorward moving polar air. The result is a net poleward motion of energy without the angular momentum following (Johnson, 1989). Additionally, there is a conversion of kinetic energy from mean zonal to eddy in the mid-latitudes to facilitate wave growth and energy transfer (Riemer and Jones, 2010).

After the energy is converted to eddy kinetic, it can then be sent downstream. The energy then becomes available to develop further jets and waves as it moves downstream, after which it can be converted back to potential energy as it exits the jets (Martin, 2014). The energy can also be used to develop a surface cyclone, as can occur due to upper tropospheric divergence in a jet's tropospheric Sawyer-Eliassen circulations that leads to lower surface pressure and rising motion through the local troposphere. If this occurs, the eddy kinetic energy is dissipated by friction at the surface, creating a small amount of heating and converting the eddy kinetic energy to internal energy (Jin et al., 2007).

2.3 The Role Of The Sawyer-Eliassen Circulations

The jet and its entrance region Sawyer-Eliassen circulation are important features that allow for the mixing out the angular momentum needed to permit poleward movement of the energy. The entrance region circulation brings tropical air parcels poleward across the jet (Uccellini and Kocin, 1987) that have high angular momentum. The high angular momentum air parcels then mix angular momentum zonally and downward into the equatorward moving polar air via pressure stresses where vertical and zonal wind shear cause mixing across the area of shear (Johnson, 1989), all while the potential energy is converted to eddy kinetic by acceleration in the entrance region and the thermally direct jet entrance region Sawyer-Eliassen circulation (Namias and Clapp, 1949). The downward portion of angular momentum transport in the mid-latitudes can be seen in a time average in Figure 3 in Widger Jr (1949) (refer to Fig. 1.2). The equatorward side vertical branches of the jet entrance region Sawyer-Eliassen circulation also help to bring down additional air parcels from the tropical upper troposphere and lower stratosphere and bring up additional air parcels from the mid-troposphere (Lang and Martin, 2013), maximizing the reach of the circulation into the high energy equatorward area (refer to Fig. 1.4). Vertical pressure stress (or stress along a horizontal plane) originates from the difference between wind in a jet core (large) and the wind at the ground (zero) (Holton, 2004). As angular momentum is far larger for the upper level air parcels brought in from the tropics than for low level air parcels in the mid-latitudes (Marshall and Plumb, 2008), any mixing of the two would lead to

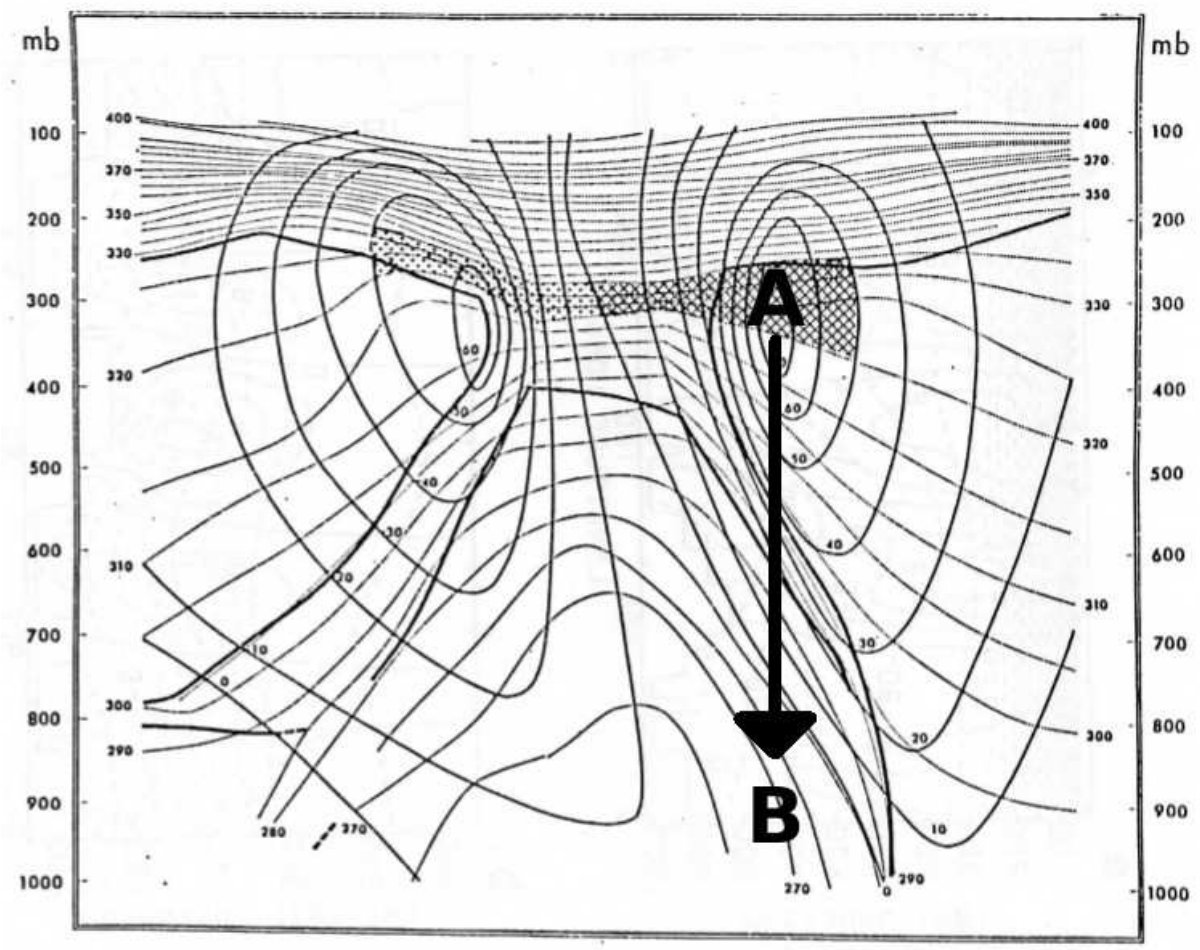

Figure 2.1: Cross-section looking north of a baroclinic wave studied by Newton and Palmén (1963), also Figure 27 (without letters or arrow) from Johnson (1989). Thinnest lines are isentropes, medium lines are isotachs of meridional wind, and thick lines are frontal boundaries and tropopause. Cross-hatched area represents poleward mass transport in the 320-335 Kelvin layer and the poleward side of the wave. Dotted area represents equatorward mass transport and the equatorward side of the wave. Vertical axis is pressure. A represents an area of tropical high-angular momentum air. B represents an area of polar low-angular momentum air. Arrow represents the transfer of angular momentum due to pressure stresses caused by the poleward-moving jet centered on A and the lower velocity equatorward-moving air below.

a reduction of angular momentum for the higher energy tropical poleward moving air parcels and a gain for the lower energy polar air parcels (Fig. 2.1).

All of the previously described motion occurs in the jet entrance region, an area typically most pronounced near the base of a trough on the poleward moving (downstream) side of the trough, as jet streaks typically form in the meridional portions of waves (Orlanski and Sheldon, 1995) due to effects of curvature on geostrophic flow creating subgeostrophic winds at the base of a trough (Martin, 2006). This can be seen at times as a break or minimum in the jet speed. This fits well with the poleward motion of mass and energy. The jet exit region also has Sawyer-Eliassen circulations, but their motions are reversed from the jet entrance circulations. The combined effect of the jet exit circulations is to create an equatorward across-jet motion (Uccellini and Kocin, 1987). The jet exit region is most pronounced near the base of a trough on the equatorward moving (upstream) side due to the same jet speed minimum or break at the base of a trough and jet streak formation in meridional portions of waves (Orlanski and Sheldon, 1995). This also aligns well with the idea of an equatorward motion of polar air. This equatorward motion would also be expected to return some smaller amount of energy and angular momentum back toward the tropics, especially if any mixing of higher energy and angular momentum air had occurred beforehand on the polar side of the wave (Yamazaki and Peltier, 2014), possibly slowing the loss of energy and angular momentum from the area equatorward of the wave.

Development of a surface cyclone can prevent this recycling of energy from occurring as efficiently as possible. A strong surface cyclone has strong low level winds associated with it, something that exposes this eddy kinetic energy to large frictional forces (Jin et al., 2007). Preventing this energy from returning to the subtropics cuts off the energy source for baroclinic waves and jets, which will eventually lead to the end of the surface cyclone as upper level divergence from the jet ends and surface convergence fills the cyclone (Martin, 2006). Instead, a frictional warming occurs and the energy is converted to internal energy in the low levels due to frictional heating, increasing Montgomery streamfunction a small amount in the low levels (Jin et al., 2007). That energy can then radiate to space from the low levels, completing the global energy balance (Dopplick, 1972).

2.4 Metrics To Describe Energy And Its Movement

Montgomery Streamfunction

In isentropic coordinates, the dry static energy is the Montgomery streamfunction. The form of Montgomery streamfunction is

$$M = C_p T + gz \quad ,$$

where C_p is the constant pressure heat capacity of air, T is the temperature in Kelvin, g is the gravitational constant, and z is the height above the surface (American Meteorological Society, 2014b). Not all of the dry static energy present is available to be converted to other forms of energy and perform work, though. Much like Available Potential Energy (Lorenz, 1955) is only a fraction of the total potential energy, one

should not expect the entire Montgomery streamfunction to be available to be converted to kinetic energy. It is possible to define a standard Montgomery streamfunction on potential temperature surfaces using the U.S. Standard Atmosphere (Atmosphere, 1976) that appears similar to a mid-latitude temperature profile. That standard Montgomery streamfunction can then be subtracted from the actual Montgomery streamfunction on a potential temperature surface to find the available Montgomery streamfunction. This Montgomery streamfunction is available in the sense that it is an anomaly from what is defined as the standard Montgomery streamfunction, which is found using an atmosphere with a tropopause at 12 kilometers (Atmosphere, 1976), similar to the mid-latitudes. This standard atmosphere can then be used as a reference extratropical sounding, and variations from this reference sounding represent energy differences between the two soundings. It is then the approximate energy available to convert the atmosphere to that standard extratropical state, just as Available Potential Energy (APE) is available to return the atmosphere to its lowest potential energy state (Lorenz, 1955). Further reasoning for the existence and usage of MAPE will be given in a later section.

In the same vein as APE, the available Montgomery streamfunction can be referred to as Montgomery Available Potential Energy (MAPE). This MAPE is in J/kg, which can be converted to J/m^3 by multiplying by the local density of air. The J/m^3 measure produces a less distorted value of MAPE at varying heights by not having extremely large J/kg values that are actually relatively low energy due to the low air

density in upper levels due to the ideal gas law

$$\rho = \frac{p}{RT} \quad ,$$

where density ρ is proportional to pressure p. Areas of high MAPE in the upper levels can be expected to be in tropical air masses due to their higher heights of isentropes (Marshall and Plumb, 2008). Larger volumes of isentropic layers, found in the upper tropical troposphere after heating (Martin, 2006) due to latent heat release (Trenberth and Stepaniak, 2003), also lead to more energy given the same area.

Eliassen-Palm Fluxes and Wave Activity

Tied to the MAPE is excess angular momentum, as angular momentum is acquired in the tropics, as described previously. The Eliassen-Palm flux is a method for determining the movement of angular momentum (Gill, 1982). The horizontal component of Eliassen-Palm flux is

$$F_x = (v')^2 - (u')^2$$

$$F_y = -u'v' \quad ,$$

where u' and v' are the perturbation from the average zonal and meridional winds, respectively (Edmon Jr et al., 1980; Trenberth, 1986). This is a movement of Rossby wave activity and is opposite to the meridional flux of angular momentum u'v'. Eliassen-Palm flux convergence (negative divergence) is also associated with increases in wave activity and amplitude, as shown by

$$\partial A / \partial t + \nabla \vec{F} = D$$

(Andrews, 1987), where A is the wave activity, t is time, F is the Eliassen-Palm vector, and D is a non-conservative source of wave activity. This flux convergence can lead to greater energy and momentum transfer due to increased meridional winds at the expense of zonal winds in an amplified wave that extends further meridionally than an unamplified wave. Wave activity A is defined as

$$A = \frac{1}{2}\rho_0 \bar{\eta}^{\prime 2} \frac{\partial \bar{q}}{\partial y} \quad ,$$

where ρ is density, η is the northward displacement of an air parcel, q is the quasigeostrophic potential vorticity, and y is positive to the north (Andrews, 1987). This equation directly relates meridional displacement in a wave to its wave activity.

Much like the energy conversion equation in the next section, an equation can be formulated using the wind and gradient of Eliassen-Palm flux to calculate the energy transfer occurring due to conservative zonal mean-eddy interaction using the Eliassen-Palm flux. This equation is

$$E_{ep} = -\rho\, \bar{u} \cdot \frac{\partial (u'v')}{\partial y} \quad ,$$

where u' and v' are as in the Eliassen-Palm flux above, u is the zonal wind, and ρ is density, with units W/m^3 describing the increase in eddy kinetic energy based on the zonal mean-eddy conversion of kinetic energy (Holton, 2004).

The Baroclinic Energy Conversion Equation

Baroclinic energy conversion is based on the total kinetic energy and the gradient of dry static energy, along with the density of the air. The energy conversion equation is similar to Equation 6.47b in Johnson (1989), but does not take into account the thickness of the layer (dp/dθ in Johnson's equation). Instead, the equation gives an energy conversion rate per unit volume. The equation is

$$E_m = -\rho \tilde{U} \cdot \nabla_\theta M \quad ,$$

where ρ is the density, U is the wind vector, and M is the Montgomery streamfunction. Positive values of E_m represent a conversion from available potential energy to total kinetic energy due to wind moving across a Montgomery streamfunction (and MAPE) gradient toward lower values, while negative values represent a conversion from total kinetic energy to potential as the wind relative to the gradient is reversed. A large gradient of dry static energy is typically associated with a similarly large gradient of geopotential height along an isentropic surface, which leads to acceleration of wind due to an implied pressure gradient (Marshall and Plumb, 2008) that produces more total kinetic energy. If advection is increasing the Montgomery streamfunction, this would lead to a greater conversion of energy as more MAPE is available (as the standard Montgomery streamfunction does not vary) assuming that the wind continues crossing the gradient. This metric also describes a poleward heat flux, as high MAPE in the tropical upper troposphere/lower stratosphere correlates with high potential temperature (a positive anomaly, refer to Fig. 1.3.). If the wind is directed away from the tropics (northward

in the northern hemisphere, a positive anomaly), these two variables create a positive correlation of v'θ'. The positive value represents a positive poleward heat flux, as v'θ' is the main component of the vertical Eliassen-Palm flux that describes poleward heat fluxes (Gill, 1982).

This equation can be derived from the Eulerian mean and eddy equations for quasigeostrophic motion. The eddy equation starts with these equations for horizontal motion (Equations 10.51 and 52 in Holton without turbulent drag forces):

$$(2.1)\quad \frac{\partial u'}{\partial t}+\bar{u}\frac{\partial u'}{\partial x}-fv'-v'\frac{\partial \bar{u}}{\partial y}=\frac{-\partial \Phi'}{\partial x} \quad \text{and}$$

$$\frac{\partial v'}{\partial t}+\bar{u}\frac{\partial v'}{\partial x}+fu'=\frac{-\partial \Phi'}{\partial y} \quad ,$$

where primes indicate eddy (perturbation) values and bars indicate zonal means, u is the zonal wind, v is the meridional wind, f is the Coriolis parameter, Φ is the geostrophic height, t is time, and x and y are zonal and meridional directions, respectively. Invoking geostrophic balance (Equation 3.26 in Holton), justified by the near-geostrophic winds observed outside the tropics (Martin, 2006) where this equation will be used, produces

$$(2.2)\quad \frac{\partial u'}{\partial t}+\bar{u}\frac{\partial u'}{\partial x}+\frac{\partial \Phi'}{\partial x}-v'\frac{\partial \bar{u}}{\partial y}=\frac{-\partial \Phi'}{\partial x} \quad \text{and}$$

$$\frac{\partial v'}{\partial t}+\bar{u}\frac{\partial v'}{\partial x}+\frac{\partial \Phi'}{\partial y}=\frac{-\partial \Phi'}{\partial y} \quad .$$

Multiplying through by u'/2 and v'/2 respectively (to allow for eddy kinetic energy to be defined in the next step) and combining like terms produces

(2.3) $$\frac{u'}{2}\frac{\partial u'}{\partial t}+\bar{u}\frac{u'}{2}\frac{\partial u'}{\partial x}+2\frac{u'}{2}\frac{\partial \Phi'}{\partial x}-(\frac{u'}{2}v')\frac{\partial \bar{u}}{\partial y}=0$$ and

$$\frac{v'}{2}\frac{\partial v'}{\partial t}+\frac{v'}{2}\bar{u}\frac{\partial v'}{\partial x}+2\frac{v'}{2}\frac{\partial \Phi'}{\partial y}=0 \quad .$$

Averaging rules lead to the multiplication of a perturbation and mean becoming zero (on the left side), with a reversing of the product rule on the right side leading to the equations becoming this:

(2.4) $$\frac{\partial(\frac{u'}{2})^2}{\partial t}+u'\frac{\partial \Phi'}{\partial x}-\frac{1}{2}(u'v')\frac{\partial \bar{u}}{\partial y}=0$$ and

$$\frac{\partial(\frac{v'}{2})^2}{\partial t}+v'\frac{\partial \Phi'}{\partial y}=0 \quad .$$

Use of the product rule on the final u'v' term gives this result:

(2.5) $$\frac{\partial(\frac{u'}{2})^2}{\partial t}+u'\frac{\partial \Phi'}{\partial x}+\frac{1}{2}\bar{u}\frac{\partial(u'v')}{\partial y}=0$$ and

$$\frac{\partial(\frac{v'}{2})^2}{\partial t}+v'\frac{\partial \Phi'}{\partial y}=0 \quad .$$

Finally, rearranging terms and multiplying through by the sea level density ρ_0 gives the eddy kinetic energy change equation in log-pressure coordinates

(2.6) $$\rho_0\frac{\partial(\frac{u'}{2})^2}{\partial t}=-\rho_0 u'\frac{\partial \Phi'}{\partial x}-\frac{1}{2}\rho_0\bar{u}\frac{\partial(u'v')}{\partial y}$$ and

$$\rho_0\frac{\partial(\frac{v'}{2})^2}{\partial t}=-\rho_0 v'\frac{\partial \Phi'}{\partial y}$$, or combined:

$$\rho_0 \frac{\partial\left(\left(\frac{u'}{2}\right)^2+\left(\frac{v'}{2}\right)^2\right)}{\partial t} = -\rho_0 \vec{U}' \nabla \Phi' - \frac{1}{2}\rho_0 \bar{u} \frac{\partial(u'v')}{\partial y} \quad .$$

The terms on the right side of the combined equation represent eddy kinetic energy conversion from eddy height gradients and from zonal mean kinetic energy, respectively.

However, the desired result is an isentropic coordinate equation, not the log-pressure coordinate equation seen here. Simply changing Φ to Montgomery streamfunction M is not possible, as Montgomery streamfunction is a function of height and temperature. This can be rectified by using the ideal gas law to change the reference density ρ_0 to an actual density ρ. The ideal gas law can be used to connect three variables if one is held constant (R is the universal gas constant). In this case, pressure p will be constant and density and temperature T will vary:

$$p = \rho_0 R T_0 \quad \text{and} \quad p = \rho R T \quad .$$

Both are equal to the constant pressure, giving this relation:

$$(2.7) \quad \rho_0 R T_0 = \rho R T \quad \text{or} \quad \rho_0 = \frac{\rho T}{T_0} \quad ,$$

after canceling the equivalent R on each side. Start at the definition of an eddy Montgomery streamfunction multiplied by the density equation 2.7:

$$(2.8) \quad \rho_0 M' = \rho_0 C_p T' + \rho_0 \Phi' \quad \text{or} \quad \frac{\rho T}{T_0} M' = \frac{\rho T}{T_0} C_p T' + \frac{\rho T}{T_0} \Phi' \quad ,$$

then break the total temperature into mean and perturbation components:

$$\frac{\rho(T_0+T')}{T_0} M' = \frac{\rho(T_0+T')}{T_0} C_p T' + \frac{\rho(T_0+T')}{T_0} \Phi' \quad ,$$

and separate the components, dividing out mean temperature T_0 when it appears in both the numerator and denominator of a fraction:

$$(2.9)\quad \left(\rho+\frac{\rho T'}{T_0}\right)M'=\left(\rho+\frac{\rho T'}{T_0}\right)C_pT'+\left(\rho+\frac{\rho T'}{T_0}\right)\Phi' \quad ,$$

and distribute the coefficients in all terms

$$(2.10)\quad \rho M'+\frac{\rho T'}{T_0}M'=\rho C_pT'+\frac{\rho T'}{T_0}C_pT'+\rho\Phi'+\frac{\rho T'}{T_0}\Phi' \quad .$$

The perturbation Montgomery streamfunction multiplied by density (each term without T_0) can be removed as all its components combined are equal to zero, along with the density itself and the common denominator T_0 left in each term:

$$T'M'=T'C_pT'+T'\Phi' \quad \text{or} \quad T'^2+\left(\frac{-M'+\Phi'}{C_p}\right)T'=0 \quad .$$

This is now a quadratic equation with the variable T' and other values being coefficients. Completing the square can be done on this quadratic equation:

$$ax^2+bx+c=0 \quad \text{becomes} \quad a(x+d)^2+e=0 \quad ,$$

$$\text{where} \quad d=\frac{b}{2a} \quad \text{and} \quad e=c-\frac{b^2}{4a} \quad .$$

As c=0 in this equation, the result of completing the square is

$$\left(T'+\left(\frac{-M'+\Phi'}{2C_p}\right)\right)^2+\left(0-\left(\frac{(-M'+\Phi')^2}{4C_p^2}\right)\right)=0 \quad .$$

Move the final term to the other side of the equal sign and take the square root:

$$T'+\frac{-M'+\Phi'}{2C_p}=\frac{-M'+\Phi'}{2C_p} \quad .$$

The two non-T' terms are equal, leaving T'=0 after they are canceled out. Going back to Equation 2.10:

$$\rho M' + \frac{\rho T'}{T_0} M' = \rho C_p T' + \frac{\rho T'}{T_0} C_p T' + \rho \Phi' + \frac{\rho T'}{T_0} \Phi' \quad ,$$

and removing the Montgomery streamfunction with T' terms gives:

$$(2.11) \quad \rho M' = \rho C_p T' + \rho \Phi' \quad .$$

With T'=0, the equation simplifies to

$$(2.12) \quad M' = \Phi' \quad .$$

The combined eddy kinetic energy equation 2.6 was

$$\rho_0 \frac{\partial \left(\left(\frac{u'}{2}\right)^2 + \left(\frac{v'}{2}\right)^2 \right)}{\partial t} = -\rho_0 \vec{U}' \nabla \Phi' - \frac{1}{2} \rho_0 \bar{u} \frac{\partial (u'v')}{\partial y} \quad .$$

Replacing ρ_0 as in 2.8 and 2.9 gives

$$\left(\rho + \frac{\rho T'}{T_0}\right) \frac{\partial \left(\left(\frac{u'}{2}\right)^2 + \left(\frac{v'}{2}\right)^2 \right)}{\partial t} = -\left(\rho + \frac{\rho T'}{T_0}\right) \vec{U}' \nabla \Phi' - \frac{1}{2} \left(\rho + \frac{\rho T'}{T_0}\right) \rho_0 \bar{u} \frac{\partial (u'v')}{\partial y} \quad .$$

Using Equation 2.12 with T'=0, the isentropic eddy kinetic energy equation is then

$$(2.13) \quad \rho \frac{\partial \left(\left(\frac{u'}{2}\right)^2 + \left(\frac{v'}{2}\right)^2 \right)}{\partial t} = -\rho \vec{U}' \nabla M' - \frac{1}{2} \rho \bar{u} \frac{\partial (u'v')}{\partial y} \quad ,$$

with the first term on the right side being the baroclinic energy conversion term E_m in eddy form and the final term half of the zonal mean-eddy conversion term E_{ep}. M' is the variation from the zonal mean M, justifying the existence of the value MAPE as a variation from the standard M. It is this anomalous Montgomery streamfunction that drives the conversion to kinetic energy and MAPE is the value of the anomalous

Montgomery streamfunction. Note that the gradient of M and M' are equal as the mean M does not change, allowing for the usage of M in the baroclinic conversion equation.

The zonal mean kinetic energy conversion equation starts with equation 10.47 in Holton without the turbulent drag force:

$$\frac{\partial \bar{u}}{\partial t} - f\bar{v} = \frac{-\partial(u'v')}{\partial y} \quad .$$

Multiplying by $\bar{u}/2$ (to get mean kinetic energy) and using the product rule gives

$$\frac{\partial\left(\frac{\bar{u}}{2}\right)^2}{\partial t} - \frac{\bar{u}}{2} f\bar{v} = \frac{-\bar{u}}{2}\frac{\partial(u'v')}{\partial y} \quad .$$

Using geostrophic balance again (as done with the eddy equation) produces

$$\frac{\partial\left(\frac{\bar{u}}{2}\right)^2}{\partial t} - \frac{\bar{u}}{2}\frac{\partial\bar{\Phi}}{\partial x} = \frac{-\bar{u}}{2}\frac{\partial(u'v')}{\partial y} \quad . \tag{2.14}$$

The zonal derivative of the zonal mean geopotential height is zero, leaving the zonal mean kinetic energy change equation multiplied by density:

$$\rho\frac{\partial\left(\frac{\bar{u}}{2}\right)^2}{\partial t} = \frac{-1}{2}\rho\bar{u}\frac{\partial(u'v')}{\partial y} \quad . \tag{2.15}$$

As the only variables in this equation are time and horizontal wind components, and density is not dependent on this equation, there is no need to convert the height coordinates. This equation shows that the zonal mean kinetic energy is only changed by its conversion to eddy kinetic energy, so any gain of total kinetic energy can only come from the baroclinic term in the eddy kinetic energy change equation.

Additionally, the isentropic eddy (2.13) and zonal mean (2.15) kinetic energy change equations can be added together to get the total isentropic kinetic energy change over time:

$$\rho\frac{\partial\left(\left(\frac{u'}{2}\right)^2+\left(\frac{v'}{2}\right)^2\right)}{\partial t}+\rho\frac{\partial\left(\frac{\bar{u}}{2}\right)^2}{\partial t}=-\rho\vec{U}'\nabla M'-\frac{1}{2}\rho\bar{u}\frac{\partial(u'v')}{\partial y}-\frac{1}{2}\rho\bar{u}\frac{\partial(u'v')}{\partial y}$$

$$\text{(2.16)}\quad \rho\frac{\partial\left(\left(\frac{\vec{U}}{2}\right)^2\right)}{\partial t}=-\rho\vec{U}'\nabla M'-\rho\bar{u}\frac{\partial(u'v')}{\partial y}\approx E_m+E_{ep}\quad ,$$

the same as adding the two energy conversion equations E_m and E_{ep} given in the beginning of this section except for the replacement of total Montgomery streamfunction with its perturbation in E_m.

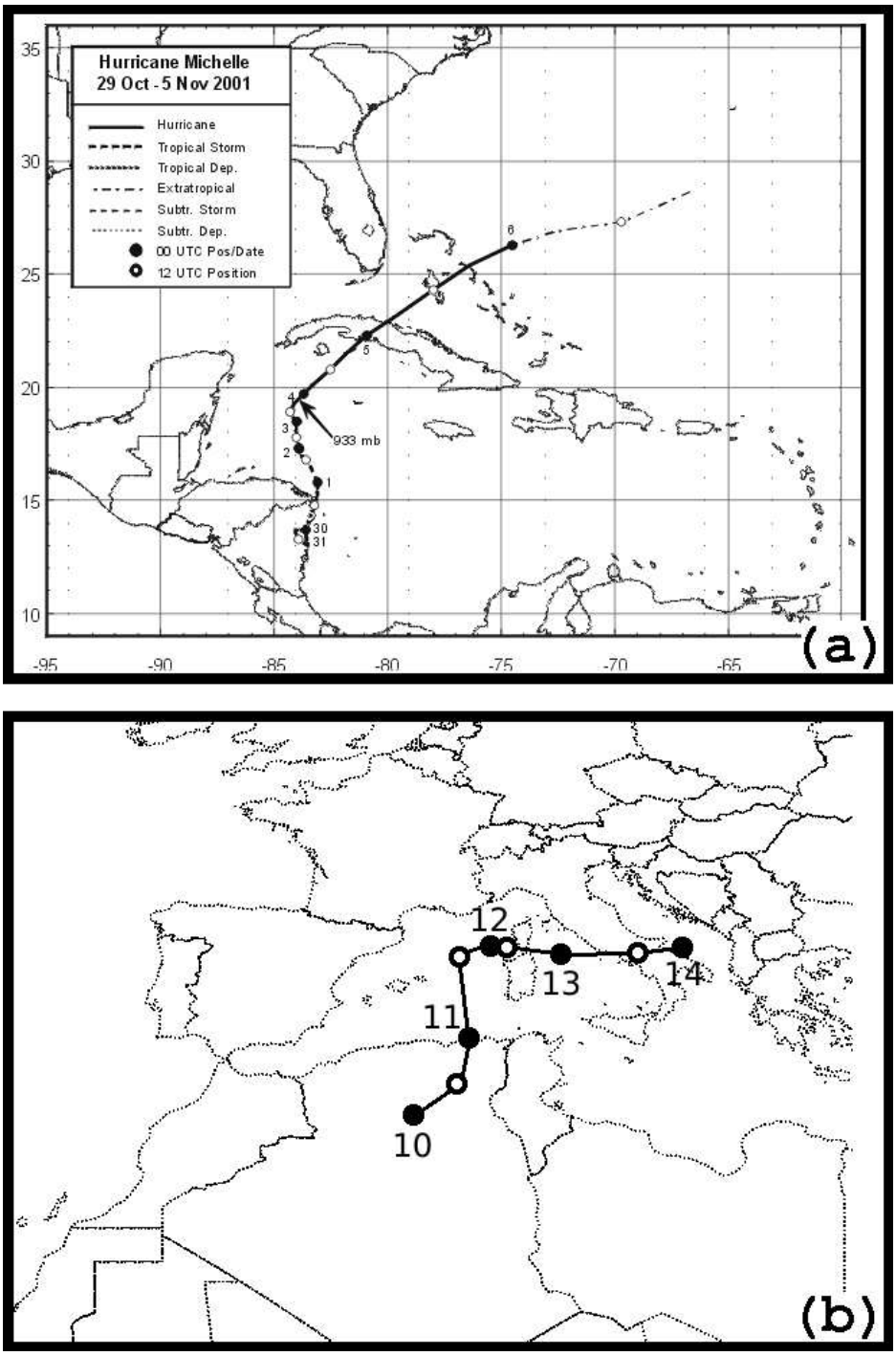

Figure 2.2: Track of (a) Hurricane Michelle in October and November of 2001 (Beven, 2002) and (b) a cyclone in the Mediterranean in November 2001. Numbers represent day of month. Cyclone track estimated from GFS surface pressure analyses.

2.5 Event Overview

The event studied occurred in late October to mid-November 2001. Category 4 Hurricane Michelle developed in the Caribbean Sea and moved northeast into the central Atlantic (Fig. 2.2a). Michelle formed on 29 Oct 2001, reached its peak intensity on 4 Nov, and was declared extratropical by the National Hurricane Center on 6 Nov. At its peak, Michelle had maximum winds of 120 knots and a minimum sea level pressure of 934 hPa (Beven et al., 2003).

A strong cyclone developed over Algeria and moved into the Mediterranean Sea (Fig. 2.2b). This cyclone first developed on 10 Nov, moved into the Mediterranean Sea on 11 Nov, and dissipated on 14 Nov. At its peak, the cyclone had a minimum sea level pressure of 989 hPa. This cyclone had extensive impacts on coastal Algeria due to its intense rainfall (Tripoli et al., 2005).

Event Details

All maps and values referenced in this section are calculated at the 345 Kelvin potential temperature level, except for the jets (at 250 hPa) and tropopause level (in kilometers). Isentropic data was interpolated from the initial GFS 1 degree by 1 degree analysis pressure-coordinate data using the GEMPAK program gdvint. All maps (except for the track maps) were created using the GEMPAK program GDPLOT and cross sections were created using GDCROSS.

The 345 K level is just above the equilibrium level (or straight isentrope) across a meridional cross-section, at the 340 Kelvin potential temperature level (Fig.

1.3). This 345 K surface is in the tropical upper troposphere and the extratropical lower stratosphere. The equilibrium level is also approximately at 250 hPa. Positive (negative) baroclinic energy conversion is defined to be conversion to (from) total kinetic energy. Negative values of Eliassen-Palm flux divergence are Eliassen-Palm flux convergence, associated with wave activity increases and increases in wave amplitude.

At 0 UTC 28 Oct, before the development of Hurricane Michelle, there was a pre-existing large scale maximum of Montgomery Available Potential Energy (MAPE) across the western Caribbean with lesser values to the east in the tropical Atlantic and to the north over the Gulf of Mexico (Fig. 2.3a). These maximum values were on the order of 3500-4000 J/m^3, with the lesser values across the tropical Atlantic being 2500-3500 J/m^3. The zero line of MAPE was seen to vary from near Iceland to north-central Quebec. While Michelle was forming, a local maximum of MAPE could be seen in the western Caribbean, such as at 18 UTC 30 Oct. This maximum was visible as the 4000 J/m^3 contour of MAPE (Fig. 2.3b), centered just north of the location of Michelle (actually Tropical Depression Fifteen at the time). At this time, the tropical cyclone was developing new convection on its north side and contained "a rather impressive outflow pattern" (National Hurricane Center, 2001a), suggesting that it was producing large amounts of upward motion, mass transport, and MAPE in the upper levels.

A local maximum of MAPE continued to exist near Michelle at 0 UTC 1 Nov. This was seen as a 4000 J/m^3 contour of MAPE in the Caribbean, compared to

2500-3000 J/m^3 background values in the tropical Atlantic (Fig. 2.3c). This enhanced MAPE production was due to especially intense convection, with cloud tops at the time nearly -90 degrees Celsius (National Hurricane Center, 2001b) (nearly 183.15 K), compared to a cold point tropopause of -84.7 degrees Celsius (188.45 K) at Riohacha, Colombia (University of Wyoming, 2001a) and -83.3 degrees Celsius (189.85 K) at San Andres Island, off the coast of Nicaragua (University of Wyoming, 2001b) at 12 UTC 31 Oct. This suggests that the convection was intense enough to reach into the stratosphere, as air parcels in the updraft continued to cool, even as the environment around it warmed due to its stratification (Sherwood et al., 2004).

This pattern of a local MAPE maximum being located near the location of Michelle continued during the time Michelle developed into a hurricane. At 12 UTC 2 Nov, a contour of 3800 J/m^3 MAPE and a tropopause height maximum were located over the center of the hurricane. Background values of MAPE across the Caribbean and tropical Atlantic were 2500-3500 J/m^3 (Fig. 2.4a). The contour of zero MAPE was located at around the latitude of far southern Greenland. The effects of this MAPE were not yet present in the subtropics or mid-latitudes, as little jet development had occurred. Little in the way of baroclinic energy conversion (Fig. 2.4b), zonal-eddy interaction energy conversion, or Eliassen-Palm fluxes (Fig. 2.4c) were present in any part of the Atlantic south of 50 degrees latitude. It was at this time that the base MAPE value was taken, as Michelle was strengthening rapidly at the time, suggestive of intense convection (Montgomery et al., 2006).

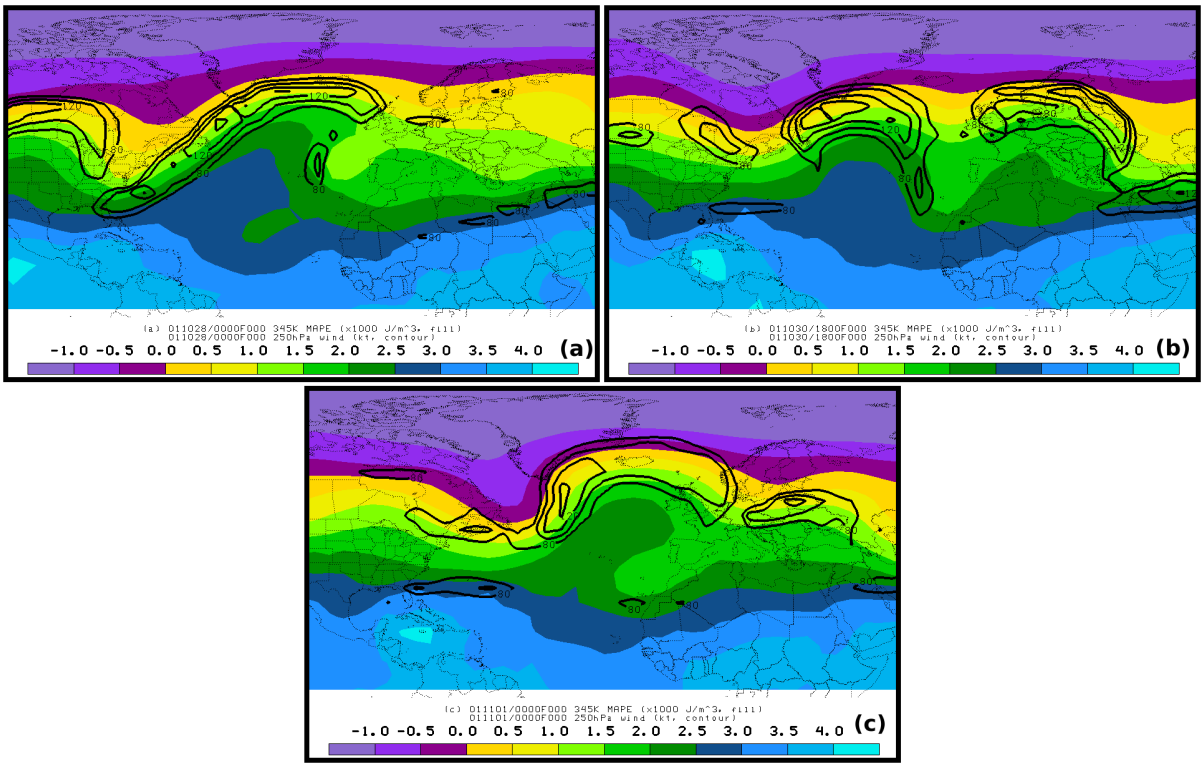

Figure 2.3: Montgomery Available Potential Energy (J/m^3) at the 345 Kelvin isentropic level (fill) and 250 hPa wind every 20 knots beginning at 80 knots (contour). (a) 0 UTC 28 Oct. (b) 18 UTC 30 Oct. (c) 0 UTC 1 Nov.

Little had changed by 12 UTC 3 Nov. The maximum of MAPE (Fig. 2.4d) and tropopause heights moved slightly north, following the path of Michelle. The maximum was a small 4000 J/m^3 MAPE contour, compared to 2500-3500 J/m^3 background values of MAPE in the tropical Atlantic. The zero MAPE line continued to be around the latitude of far southern Greenland. There was no strong gradient of MAPE at this time, precluding any development of a jet. Again, baroclinic energy conversion (Fig. 2.4e) and Eliassen-Palm fluxes (Fig. 2.4f) were very small at this time. A trough was present over Manitoba at lower tropopause levels, the precursor to a developing feature with which Michelle's energy would interact.

Activity had begun picking up by 12 UTC 4 Nov. Hurricane Michelle and its local MAPE maximum had moved little by this point, still located in the western Caribbean (Fig. 2.4g). The local maximum was a 3800 J/m^3 MAPE contour, compared to 2500-3500 J/m^3 background MAPE in the tropical Atlantic. However, the zero MAPE contour had pushed south across northern Quebec, forcing a stronger gradient of MAPE across the northeastern United States and a secondary gradient off the southeastern United States coast. The stronger gradient had forced the development of a 100 knot jet off the southeastern United States coast, along with small areas of baroclinic energy conversion on each end (Fig. 2.4h). An area of weak positive baroclinic energy conversion near the coast of Georgia and the Carolinas and a small area of weak negative baroclinic energy conversion on the east end of the jet had developed in response. Likewise, small areas of zonal-eddy energy convergence were present around the jet, but with far smaller values than the baroclinic conversion. While there were no contours of Eliassen-Palm flux convergence or divergence at this time (Fig. 2.4i), small magnitude Eliassen-Palm flux vectors were pointing southeastward in the entrance region, signifying some angular momentum moving northwestward (opposite to the vector). At 18 UTC, a small area of Eliassen-Palm vector convergence had developed in the entrance region, representing an increase in wave activity (not shown).

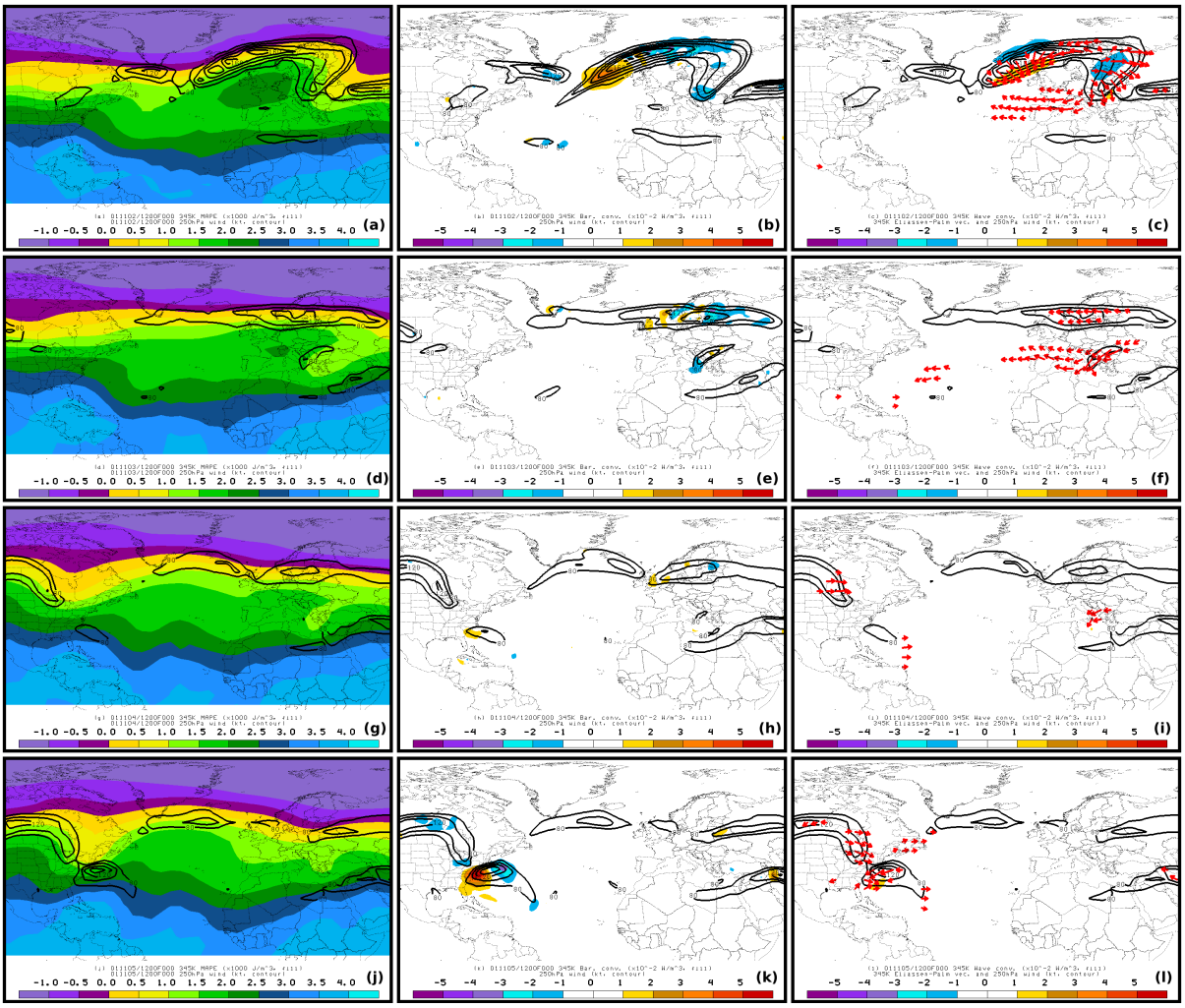

Figure 2.4: 12 UTC 2 Nov. (a) Montgomery Available Potential Energy at the 345 Kelvin isentropic level (x10^3 J/m^3, fill) and 250 hPa wind speed every 20 knots beginning at 80 knots (contour). (b) Baroclinic energy conversion at the 345 Kelvin isentropic level (x10^{-2} W/m^3, fill). Contour same as (a). (c) Zonal-eddy energy conversion (x10^{-2} W/m^3, fill) and horizontal Eliassen-Palm flux vectors at the 345 Kelvin isentropic level. Contour same as (a). Small magnitude vectors are omitted for clarity. (d-f) 12 UTC 3 Nov. (g-i) 12 UTC 4 Nov. (j-l) 12 UTC 5 Nov.

The magnitude of the MAPE gradient off the Mid-Atlantic coast had become much larger by 12 UTC 5 Nov. The zero MAPE contour remained over northern Quebec, but lower values were forming a trough over the northeastern United States (Fig. 2.4j). The maximum of MAPE was located near the Bahamas, just east of

Michelle's location. This was likely caused by southwesterly shear stopping westward movement of high energy outflow from the hurricane's convection (National Hurricane Center, 2001c). The more intense gradient was manifesting itself as a 140 knot jet off the Mid-Atlantic coast. This stronger jet had intense baroclinic energy conversion associated with it, as a large area of highly positive baroclinic energy conversion had developed in the jet entrance region in the Mid-Atlantic states, with large areas of highly negative baroclinic energy conversion on the jet's exit region in its east end (Fig. 2.4k). Zonal mean-eddy kinetic energy conversion had also grown significantly with positive conversion on the south side of the jet and negative on the north side, but was still far less than the baroclinic conversion. Eliassen-Palm fluxes were also larger at this time, with vectors pointing southeastward in the entrance region (Fig. 2.4l). These vectors were causing Eliassen-Palm flux convergence in the right entrance region of the jet (on its south side), while divergence was occurring in the left entrance region (on its north side). This moves more wave activity to the south side of the jet, suggesting a deepening of the trough.

Additionally, the downward movement of angular momentum in the jet core can be seen in a cross section through the jet (Figure 2.5a). Negative values of u'w', a vertical transfer of horizontal momentum (Kuo et al., 2008), are present extending from the lower part of the jet to the surface and in the upper core of the jet, representing a downward movement of angular momentum out of the jet itself and the high energy upper tropospheric/lower stratospheric air, respectively. Additionally,

a higher value of angular momentum was present at the 345 K level in the polar air north of the jet compared to the same latitude elsewhere—a maximum that was not strongly present 24 hours earlier, before the development of the jet (Figure 2.5c and d). This suggests that the extra angular momentum originating in the tropics was being mixed into this polar air.

The maximum of MAPE had moved north at 12 UTC 6 Nov. At this point, the 1800 J/m^3 contour of MAPE was east of the Caribbean, with anomalously high MAPE values of 2500 J/m^3 pushing as far north as 40 degrees latitude over the

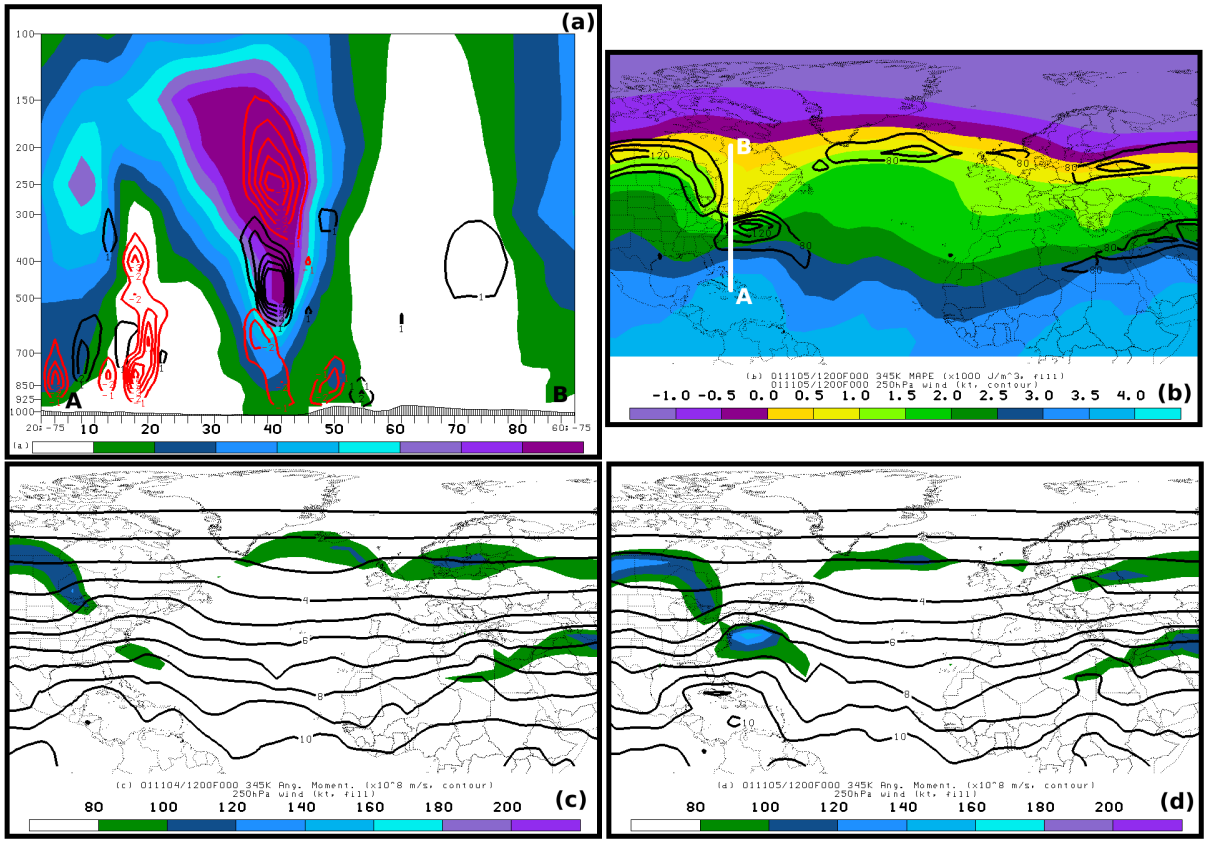

Figure 2.5. (a) Cross-section (labeled in (b)) of zonal wind (fill) and u'w' (contour) at 12 UTC 5 Nov 2001. Positive (negative) u'w' is black (red). (b) Same as 2.3j, but with line to mark cross-section in (a). (c) 250 hPa wind (fill) and 345 K angular momentum (contour) at 12 UTC 4 Nov. (d) Same as (c), but for 12 UTC 5 Nov.

west-central Atlantic and the zero MAPE line pushing into south-central Greenland (Fig. 2.6a). The area of low MAPE associated with the trough over the United States had moved off the Mid-Atlantic coast and slightly south, forcing an even stronger gradient of MAPE that was now tilted northwest to southeast. The result was a continued strong 120 knot jet off the Atlantic coast of the United States and Canada. Large areas of positive baroclinic energy conversion were present in the several areas of accelerating flow on the southwest end of the jet, while a large area of negative baroclinic energy conversion was present in the exit region of the jet over maritime Canada. Additionally, a 140 knot jet and associated baroclinic energy conversion contours had developed from Greenland to the British Isles (Fig. 2.6b), as anomalously high MAPE values of 1000-1500 J/m^3 at high latitudes of around 50 degrees created a north-south MAPE gradient in these areas. Zonal-eddy energy conversion had decreased at this time, but the pattern of positive and negative conversion across the jet remained. Eliassen-Palm flux vectors were also present in the jet, with larger vectors pointing southeastward across the entrance regions (Fig. 2.6c). Eliassen-Palm flux convergence was seen southeast of the jet off the northeastern United States coast, with strong divergence northwest of the jet closer to the coast. This suggests that wave activity would grow east of the jet, but decay strongly west of the jet, meaning that it is likely for the wave to decay after this point, which it did for a short time. There was little Eliassen-Palm flux in the exit region, suggesting that angular momentum was mostly moving northwest across the jet. There was also little zonal-eddy energy conversion or Eliassen-Palm flux across the

jet near Greenland due to the zonal nature of the jet at this time.

A noticeable ridge of MAPE was present at 12 UTC 7 Nov. The zero MAPE line was moving north through Greenland at this time with near-tropical values of 2500 J/m^3 of MAPE crossing 45 degrees latitude in the central Atlantic. For reference, the zero MAPE contour was around 50 degrees latitude elsewhere in the map (Fig. 2.6d). A strong gradient of MAPE arched from near Bermuda through

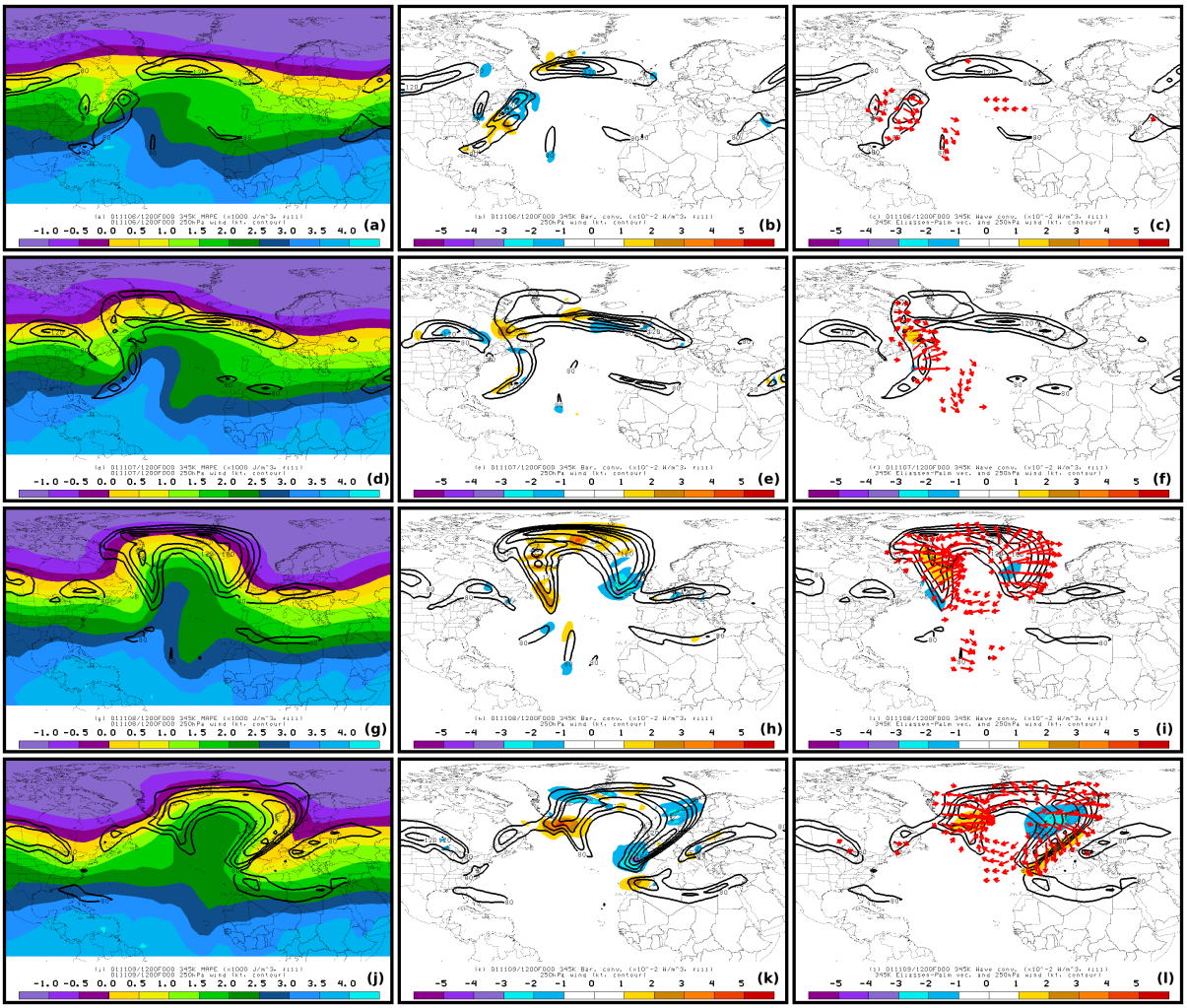

Figure 2.6: Same as Fig. 2.3, but for (a-c) 12 UTC 6 Nov. (d-f) 12 UTC 7 Nov. (g-i) 12 UTC 8 Nov. (j-l) 12 UTC 9 Nov.

Newfoundland to the north-central Atlantic. A jet ranging from 100 to 140 knots was located near this gradient. The most intense positive baroclinic energy conversion with this jet was located near Labrador and between Iceland and Greenland. The most intense baroclinic negative energy conversion was located south of Iceland, just downstream of the 140 knot jet maximum (Fig. 2.6e). Weaker baroclinic energy conversion continued to be located with the jet off the United States coast. However, the jet off the United States coast was the location of the largest zonal-eddy energy conversion and Eliassen-Palm fluxes, due to its north-south orientation creating a large meridional flux of zonal momentum. However, these values were still less than the baroclinic conversion. In the core of that jet, large Eliassen-Palm flux vectors were pointed northeast across the jet. This led to large values of Eliassen-Palm flux divergence in the west (polar) side of the jet and convergence in the east (tropical) side (Fig. 2.6f). Again, as the rest of the jet complex was oriented zonally, little Eliassen-Palm flux was occurring with that portion.

Anomalously high values of MAPE continued to push northward at 12 UTC 8 Nov. The zero MAPE contour was in central Greenland at this time (Fig. 2.6g). This contour was at 45 to 50 degrees latitude outside of this ridge. Anomalously high MAPE values of 2000 J/m^3 were approaching 60 degrees latitude. A strong gradient of MAPE in the northern semicircle of the MAPE maximum in the north Atlantic was associated with a strong 120 to 160 knot jet stretching from near Newfoundland across Greenland to near the British Isles. Massive areas of positive baroclinic energy conversion in the western two-thirds of the jet and a large area of negative

baroclinic energy conversion west of the British Isles represented the massive amounts of energy being converted to maintain this jet (Fig. 2.6h). The large areas of strong meridional wind also led to intense zonal-eddy energy conversion and Eliassen-Palm fluxes in the jet, especially in the entrance region. Positive zonal-eddy energy conversion was seen on the east (tropical) side of the entrance region, with negative conversion on the west (polar) side. A multitude of large magnitude Eliassen-Palm flux vectors pointed eastward across the western half of the jet into the tropical air (Fig. 2.6i). A large and intense couplet of Eliassen-Palm flux divergence (to the west) and convergence (to the east) were also present. This represented a massive growth in wave activity on the east side of the jet, with a decay to the west. This also represented a massive movement of angular momentum from the high energy area to the trough west of it. In the east side of the jet, the opposite occurred. Eliassen-Palm flux vectors pointed into the trough to the east, leading to weaker and smaller areas of Eliassen-Palm flux divergence (to the west) and convergence (to the east). This represented a smaller, but still significant, movement of angular momentum from the trough to the ridge and a likely growth of the trough due to its increased wave activity.

A local maximum of MAPE had developed in the north Atlantic by 12 UTC 9 Nov as a contour of 2400 J/m^3 of MAPE had closed off. The contour of zero MAPE was located well north of Iceland, with the 2400 J/m^3 maximum just to the south (Fig. 2.6j). A strong MAPE gradient extended from near Iceland through the British Isles and down to northern Africa. A strong 120 to 160 knot jet continued to wrap around

the top of the ridge defined by this anomalous MAPE. Another 100 knot jet was also forming over northern Africa, which would become important as the surface low developed. Baroclinic energy conversion associated with the northern jet was still occurring (Fig. 2.6k), though the areas of negative baroclinic energy conversion scattered through the jet appeared to be larger than the areas of positive baroclinic energy conversion in the jet entrance region, suggesting that this jet will decay. The jet over Africa, however, had a large area of positive baroclinic energy conversion with small areas of negative baroclinic energy conversion, so it would be expected to strengthen. The zonal-eddy energy conversion and Eliassen-Palm fluxes were all located in the northern jet. The pattern of Eliassen-Palm vectors entering the ridge in the west side and exiting on the east continued, along with the Eliassen-Palm flux divergence and convergence patterns seen 24 hours earlier (Fig. 2.6l), though the magnitudes of divergence and convergence were equal on both sides of the ridge. Angular momentum was expected to move out of the ridge on its west side and re-enter on its east side. Zonal-eddy interactions grew as well, with larger couplets of positive and negative values across the jet. The magnitude of the zonal-eddy energy conversion was high across much of the northern jet, with negative conversion in the midsection of the jet and positive areas mostly toward the ends. The exit region positive area was also approaching the jet over Africa.

Vertical angular momentum transfer was even larger at this time than previously. Very large negative values of u'w' were present over the higher terrain of Greenland (Fig. 2.7a), representing large movement of momentum downward into these mountains. The area of the MAPE maximum is also a local zonal angular momentum minimum (Fig. 2.7c and d), again a result of the extraction of angular momentum from that area. This loss of momentum can be explained by the higher terrain of Greenland allowing for stronger westerly surface winds that lead to a loss of momentum from the low levels (Lilly et al., 1982), leaving low momentum air to

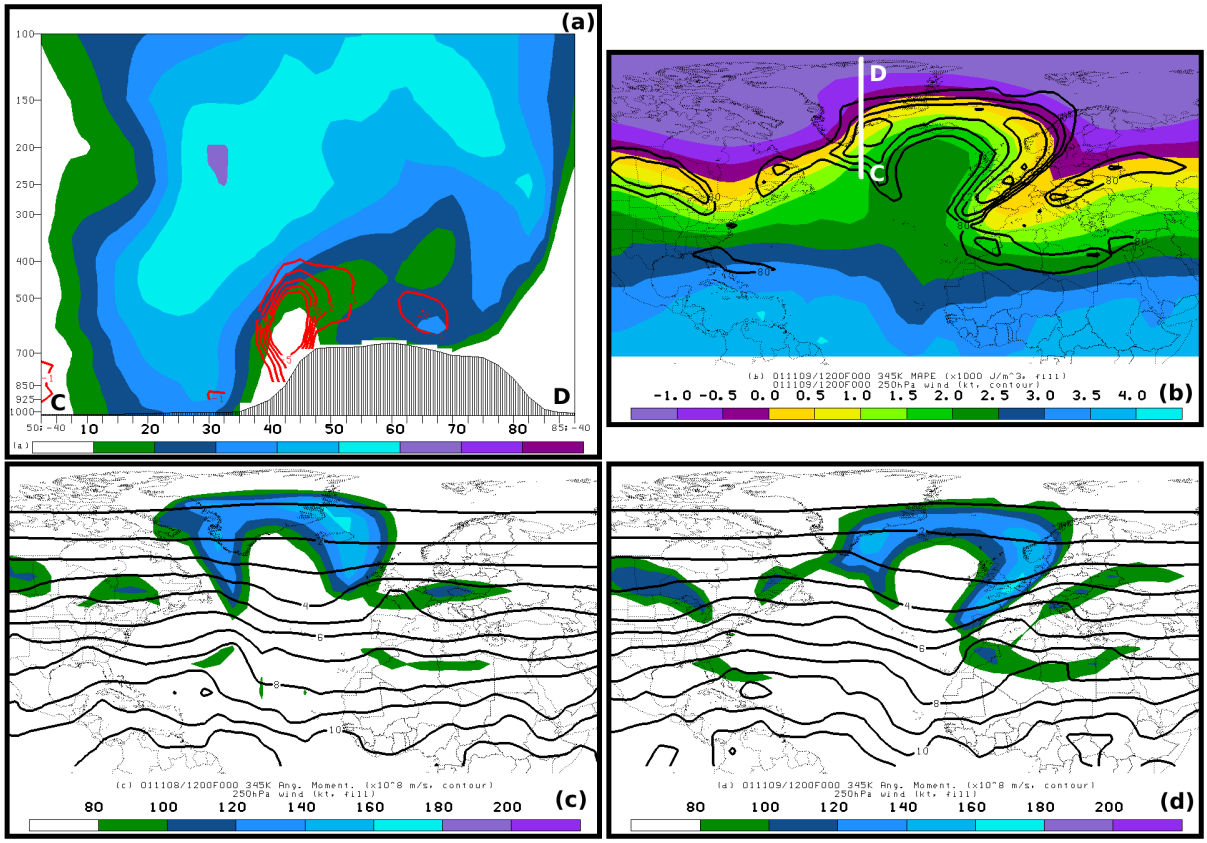

Figure 2.7. (a) Same as Fig. 2.4a, but for cross-section indicated in (b) at 12 UTC 9 Nov. (b) Same as 2.5j, except with line to indicate location of cross-section in (a). (c) 250 hPa wind (fill) and 345 K angular momentum (contour) at 12 UTC 8 Nov. (d) Same as (c). but for 12 UTC 9 Nov.

mix with higher momentum air above and transferring that momentum downward. Also noteworthy was a strong windstorm that occurred in Iceland around and after this time associated with the strong jet streak in the amplified wave train (Ólafsson and Shapiro, 2002; Shapiro et al., 2002).

The strongest gradient was pushing to the southeast side of the MAPE maximum by 12 UTC 10 Nov. The maximum still contained a closed contour of 2400 J/m^3, but it was moving back south at this point, located off the coast of Portugal (Fig. 2.8a). The strongest gradient extended from France to northwestern Africa and east into the eastern Mediterranean. This was reflected in the jet strengths, as the strongest separate 140 knot jets were over Spain and Algeria, divided by the base of a trough over the Mediterranean. A 120 knot jet extended north of the ridge, over Greenland and Iceland. Baroclinic energy conversion was strongest with the 140 knot jets, though the areas in the Spanish jet were small (Fig. 2.8b). The Algerian jet continued to have a larger area of positive baroclinic energy conversion than negative. The pattern of positive and negative baroclinic energy conversions with the northern jet corresponded to the scattered local maxima. Zonal-eddy energy conversion was strongest and positive near the base of the trough, though these values were still far less than the baroclinic conversion. Eliassen-Palm fluxes were strongest with the Spanish jet, as the northern and Algerian jets were mostly zonal. Eliassen-Palm fluxes pointed southeastward into the trough from the ridge, and lesser magnitude fluxes pointed southeastward out of the trough. Smaller and weaker areas of convergence (in the trough) and divergence (west of the trough)

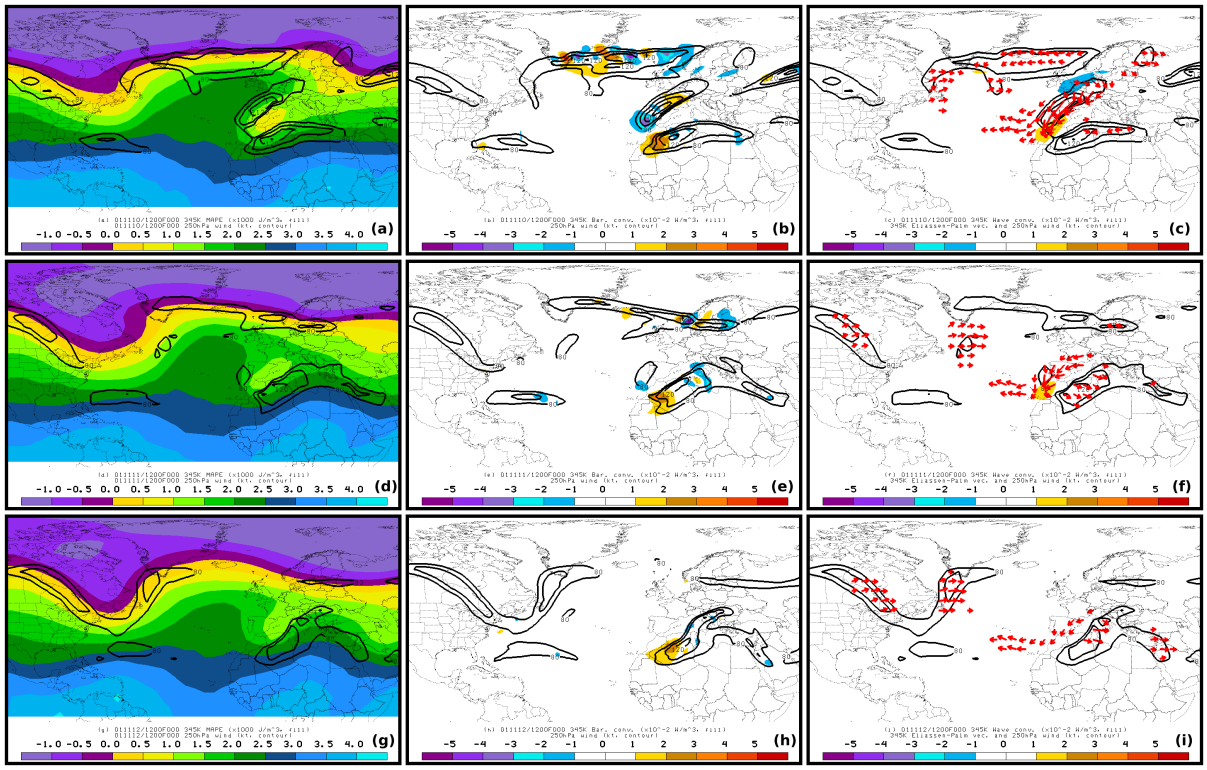

Figure 2.8: Same as Fig. 2.3, but for (a-c) 12 UTC 10 Nov. (d-f) 12 UTC 11 Nov. (g-i) 12 UTC 12 Nov.

were present, signifying the trough gaining wave activity. Angular momentum was leaving the trough for the ridge by this point, and there was no significant angular momentum leaving the ridge (Fig. 2.8c).

The MAPE gradient was shifting fully into Africa at 12 UTC 11 Nov and the local MAPE maximum moved back south into an area where it corresponded to the background MAPE (Fig. 2.8d). The zero MAPE contour was also moving back south, located through Iceland. The only jet still not in full decay was the Algerian jet. The other two jets had almost lost their identities, having a strength of 100 knots (northern jet) and 80 knots (Spanish jet). This also reflected in the baroclinic energy conversion, as both weaker jets had smaller areas of energy conversion while the

Algerian jet continued to have larger areas of baroclinic energy conversion (Fig. 2.8e). Zonal-eddy energy conversion and Eliassen-Palm fluxes also reflected this change, as the only notable fluxes were in the base of the trough and in the Algerian jet. The conversion was strongest in the base of the trough and minimal elsewhere. The Eliassen-Palm flux vectors all pointed southeastward, reflecting a northwestward motion of angular momentum, now directed toward the trough. Weak areas of Eliassen-Palm flux convergence and divergence also suggested little change in the strength of the trough (Fig. 2.8f).

The MAPE maximum had faded back into its background state by 12 UTC 12 Nov. The zero MAPE contour had also receded back to a similar latitude it was before Hurricane Michelle affected it (Fig. 2.8g). There was still a small area of strong MAPE gradient over northern Africa, and this is where the Algerian jet persisted. The other jets had weakened below perceptibility by this point, leaving only the Algerian jet to have any baroclinic energy conversion associated with it (Fig. 2.8h), though it was this jet that provided upper level divergence for the surface cyclone. Zonal-eddy energy conversion and Eliassen-Palm fluxes had also weakened back to a lowered state by this point, with the only weak vectors pointed southeastward across the Algerian jet and small areas of energy conversion in the Algerian jet. A weak couplet of divergence (to the northwest) and convergence (to the southeast) was located in the jet (Fig. 2.8i), suggesting little change in the strength of the trough or ridge the jet is between. Angular momentum movement is small and to the northwest, into the trough by this point.

2.6 Numerical Results

The maps shown previously were produced for a single level. The calculations done in this section are for the 300 to 370 Kelvin layer for MAPE and the entire 290 to 400 Kelvin layer for energy conversion by taking the values of MAPE and energy conversion for each level and adding all relevant levels together. MAPE was calculated in the 300 to 370K layer because values above 370K were unavailable. Values above 360K were significantly less than below 360K, so this omission should not have a major impact on the calculations.

The time 12 UTC 2 Nov was chosen based on the strengthening of Michelle. The smallest box, bounded by 5N, 96W, 36N, and 71W (Fig. 2.9), was used to calculate MAPE. The middle box, bounded by 5N, 90W, 51N and 50W, is the domain for energy conversion from 12 UTC 2 Nov to 18 UTC 5 Nov. The jets caused by the energy were in the domain during that time frame, but at the end of this time the jets caused by the energy expanded past this first domain. The large box, bounded by 5N, 90W, 83N, and 48E, contains the jets and associated energy conversion from 0 UTC 6 Nov to 18 UTC 11 Nov. By 0 UTC 12 Nov, the energy conversion was effectively over as none of the jets left were particularly strong.

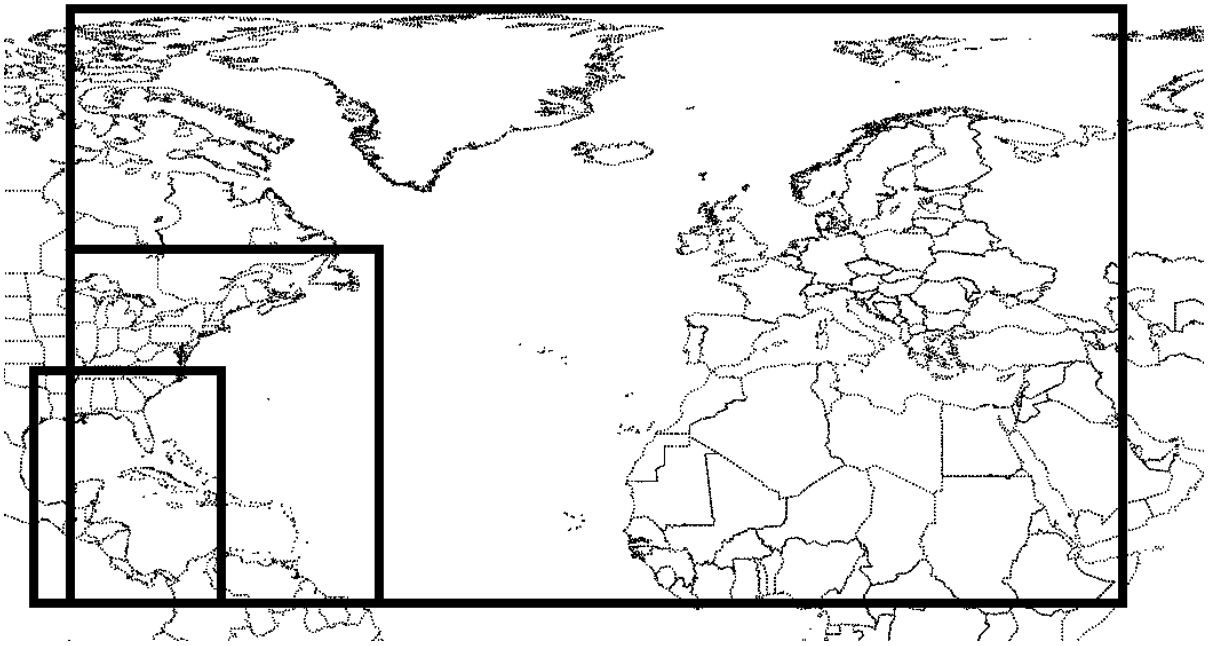

Figure 2.9: Domains for energy calculation. Small domain is for Montgomery Available Potential Energy calculation at 12 UTC 2 Nov. Medium domain is for energy conversion calculation from 12 UTC 2 Nov to 18 UTC 5 Nov. Large domain is for energy conversion calculation from 0 UTC 6 Nov to 18 UTC 11 Nov.

Conversion from Joules per cubic meter to Joules required the MAPE and energy conversion values to be multiplied by the meridional length in each grid cell (1 degree, or 111320m), the zonal length (1 degree, or 111320m divided by the zonal scaling due to the convergence of longitude lines at the poles), and the height (the height of the bottom of the layer subtracted from the top). The energy conversions also required multiplication by 21600s (or 6 hours) to convert from Watts (Joules/sec) to Joules over each 6 hour time frame and each 6 hour interval was added to get the values given here. The MAPE present at 12 UTC 2 Nov in the smallest domain was 6.4×10^{20} J. The baroclinic energy converted throughout the event was 7.5×10^{20} J. The zonal-eddy energy conversion throughout the event was

$5.0x10^{20}$ J. The baroclinic energy conversion was dominant over much of the event, starting at around double the zonal-eddy energy conversion, but zonal-eddy conversion grew to a small majority of energy conversion by 11 Nov as the baroclinic energy decayed (Fig. 2.10).

Accounting for the thickness of MAPE containing layers also provides a measure of the energy transfer. Multiplying the MAPE in a layer by its thickness gives how much MAPE per unit area is in the layer, allowing for comparison of energy in layers that have different relative energies. In this event, a pre-interaction time of 0 UTC 1 Nov was chosen, as this was when the 340 K layer was thickest in the domain around Michelle (and contained the most mass). A post-interaction time of 12 UTC 9 Nov was chosen, as this was when the amplitude of the mid-latitude Rossby wave train was greatest in the large domain, meaning it contained the most potential energy at this time.

Pre-interaction, the average thickness of the 340 K layer in the domain around Michelle was 1745m. The average variance along a zonal line from a zonal average of the tropopause was 619m, indicating a lower-amplitude lesser-potential energy containing wave train. Zonal values were chosen to prevent inter-latitudinal comparisons, such as the comparing the variance of the highly amplified mid-latitudes with the less amplified low latitudes. At this time, the average MAPE in the 345 K layer around Michelle was 3873 J/m^3, with 1987 J/m^3 in the large domain. Post-interaction, the thickness of the 340 K layer in the domain around Michelle was 1216m, a decrease of 30.3%. For the large domain, the average variance along a

zonal line from a zonal average of the tropopause was 1311m, a 52.8% increase. The lesser change in the tropical layer thickness is offset by the higher MAPE, as multiplying the MAPE with that change gives a loss of 1049 J/m^2, compared to a gain of 1174 J/m^2 in the large domain including the newly amplified mid-latitude Rossby wave train. These numbers are close, suggesting that a vast majority of the energy used in amplifying the mid-latitude Rossby wave train came from the domain around Michelle in the tropics.

Total kinetic energy also grew in the domains until 9 Nov, nearly quadrupling from 6 Nov to 9 Nov in the large domain despite an apparent lag in the kinetic energy growth. This can be seen as the line in Fig. 2.10. This shows mathematically the wave amplification seen in the maps previously.

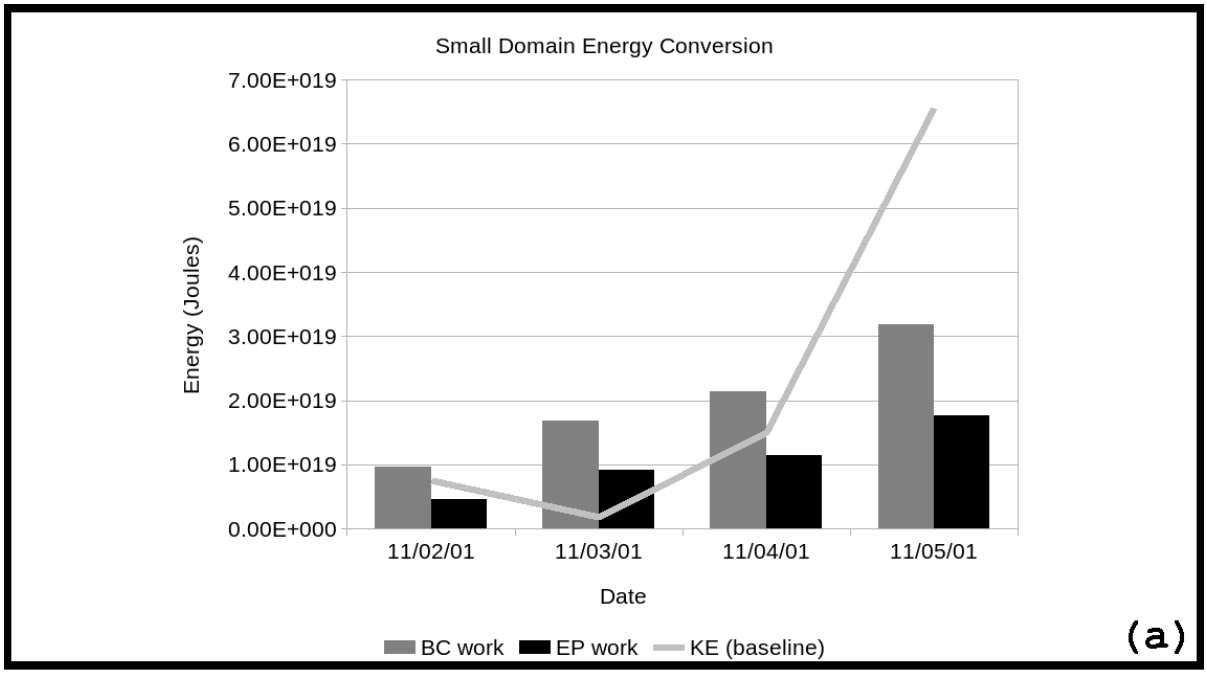

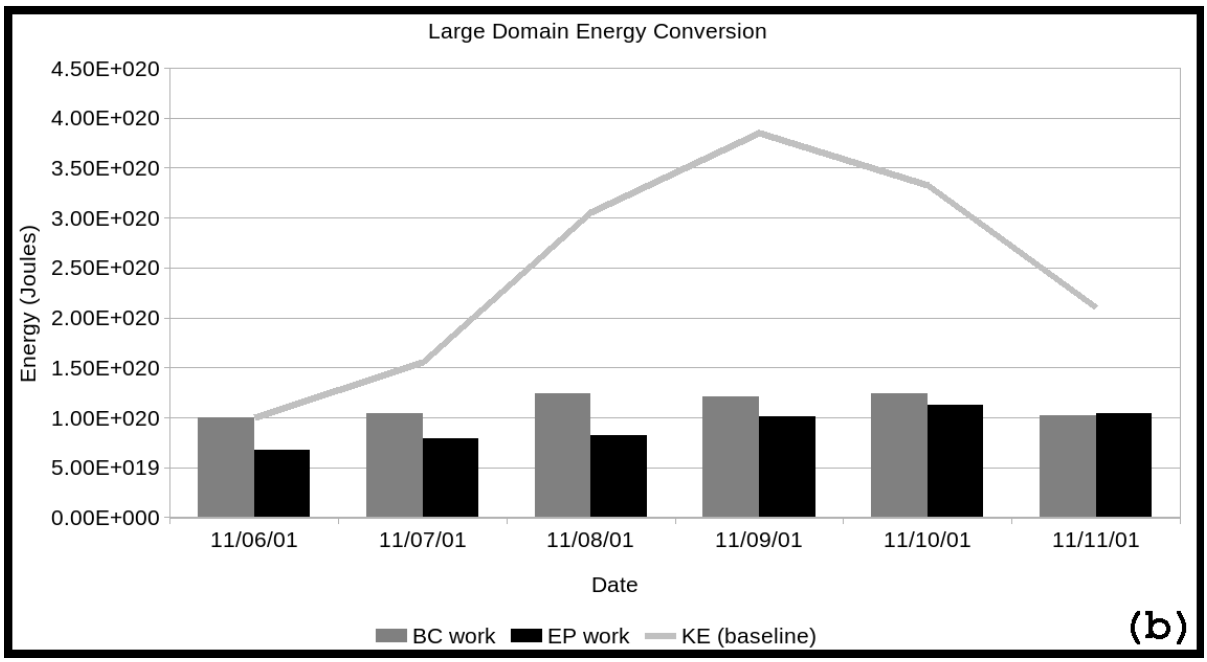

Figure 2.10: Chart of energy conversion from 290 Kelvin to 395 Kelvin isentropic levels in Joules. Horizontal axis is date. Vertical axis is energy converted (present) each day for bars (line). Gray bars are baroclinic energy conversion. Black bars are zonal-eddy energy conversion. Line is total kinetic energy. (a) is for the small domain from 2 Nov to 5 Nov. (b) is for the large domain from 6 Nov to 11 Nov.

2.6 Conclusions

A case study was performed demonstrating the connection between energy in the vicinity of Hurricane Michelle (some of which was produced by the hurricane) and a Rossby wave that was associated with the development of a strong cyclone over the Mediterranean (Tripoli et al., 2005). This connection was investigated using several metrics.

A definition of energy was calculated using Montgomery Available Potential Energy (MAPE), an anomaly of Montgomery streamfunction (dry static energy) on isentropic surfaces from the Montgomery streamfunction in the U.S. Standard Atmosphere. This calculation showed enhanced isentropic energy in the tropics and even larger values of isentropic energy around the hurricane. An equation for the baroclinic conversion of MAPE to total kinetic energy was given as a function of the wind crossing the gradient of Montgomery streamfunction, which highlighted large areas of strong baroclinic energy conversion from potential to total kinetic energy in the entrance region of jet streaks, especially in areas of a large MAPE gradient. An equation using Eliassen-Palm fluxes in place of Montgomery streamfunction was given to calculate the conversion to kinetic energy from zonal mean-eddy conversion.

A calculation of these metrics showed that the kinetic energy conversion from MAPE was greater than that due to zonal-eddy conversion, a difference that was especially large early in the event and went to zero as MAPE decreased over time. The conversion was due to the interaction of MAPE with baroclinic waves, a process

that also removes excess angular momentum, allowing high MAPE air parcels to escape the tropics.

This study confirms the qualitative notion that potential energy injected into the upper troposphere/lower stratosphere (UTLS) by tropical cyclones can be directly injected into the Rossby wave train. It further demonstrates how potential energy stored in the elevated tropical tropopause can be transferred into the extratropical Rossby wave train. These results quantitatively link the intensity of an extratropical wave event to a single tropical event. However, it follows that the entire tropical upper troposphere/lower stratosphere represents a “cache” of tropical MAPE that is available for extratropical transition given the right conditions.

Furthermore, this release of energy demonstrates the isentropic Hadley cell that connects the tropics to the extratropics. The connection between the tropics and extratropics via the isentropic Hadley cell is the pathway to inject tropical UTLS energy into mid-latitude Rossby wave trains, further demonstrating the global energy circulation extending across each hemisphere outside the traditional isobaric Hadley cell.

Chapter 3

3.1 Future Work

Extratropical transition (ET), a frequent component of the energy transfer investigated in this paper, is an event that is not well-handled by numerical weather prediction models at this point. The effect of ET on numerical models is to increase ensemble spreads, which is reflected in lower confidence forecasts from the model output (Jones et al., 2003; Harr et al., 2008).

A better understanding of the energy transfer in ET and other events where energy moves out of the tropics may lead to better numerical model output at these times. The character of the effect of ET is impacted by the tropical cyclone's strength, direction of movement, and position relative to the mid-latitude wave train (Grams et al., 2013; Riemer and Jones, 2010). Presumably, these effects would also occur in areas of MAPE not attached to tropical cyclones. Based on this, an analysis of the character of the energy transfer as a function of the above variables may provide insight into how numerical weather prediction can be improved at times during and after these energy transfers.

This could be done by creating analog sets of energy transfer events that lead to similar effects on the mid-latitudes (such as the development of certain strength jets, the release of a certain amount of energy, or a particular amplification of the mid-latitude Rossby wave train) and comparing the expected outcome of a new event based on these analogs to the actual outcome.

Another avenue for future research of this energy transfer is in the context of a changing climate. Current predictions of future climate include warmer temperatures at the low levels (Solomon, 2007), but a lifting and cooling of the stratosphere based on the warmer surface temperatures (Thuburn and Craig, 1997). The increased convection expected from this (due to warmer SSTs (Chimonas and Rossi, 1987)) is expected to strengthen positive MAPE, leading to more energy being available to convert to kinetic, creating more and/or stronger jets and waves. Additionally, the effect of a changing climate in the mid-latitudes on baroclinic waves is another variable that demands further investigation.

The magnitude of the effect of a modified climate and associated expected new vertical temperature profile on MAPE production and conversion could then be compared to the magnitudes of MAPE production and conversion changes due to other causes, such as differing atmospheric aerosol concentration (affecting the absorption and reflectivity of incoming shortwave radiation) and varying solar output. If such changes can be properly calculated, a better idea of possible future weather patterns will then be available based on possible values of the previously mentioned variables.

References

American Meteorological Society, 2014a: "dry adiabatic lapse rate." Glossary of Meteorology. [Available online at http://glossary.ametsoc.org/wiki/Dry_adiabatic_lapse_rate].

American Meteorological Society, 2014b: "dry static energy." Glossary of Meteorology. [Available online at http://glossary.ametsoc.org/wiki/Dry_static_energy].

Andrews, D. G., 1987: On the interpretation of the Eliassen-Palm flux divergence. Quart. J. Roy. Meteor. Soc., **113,** 323–338.

Anthes, R. A. and D. R. Johnson, 1968: Generation of available potential energy in Hurricane Hilda (1964). Mon. Wea. Rev., **96**, 291.

Atmosphere, U. S., 1976: National Oceanic and Atmospheric Administration. National Aeronautics and Space Administration, United States Air Force, Washington, DC.

Beer, T., G. K. Greenhut, and S. Tandoh, 1977: Relations between the Z criterion for the subtropical high, Hadley cell parameters and the rainfall in northern Ghana. Mon. Wea. Rev., **105**, 849–855.

Beven, J. L., S. R. Stewart, M. B. Lawrence, L. A. Avila, J. L. Franklin, and R. J. Pasch, 2003: Annual summary: Atlantic hurricane season of 2001. Mon. Wea. Rev., **131**, 1454–1484.

Beven, J. L., 2002: Tropical Cyclone Report: Hurricane Michelle. [Available online at http://www.nhc.noaa.gov/2001michelle.html].

Black, M. L., R. W. Burpee, and F. D. Marks Jr., 1996: Vertical motion characteristics of tropical cyclones determined with airborne Doppler radial velocities. J. Atmos. Sci., **53**, 1887–1909.

Burger, A. P., 1988: Static stability and vertical velocity: from planetary to small scale. Tellus A, **40**, 353–357.

Chimonas, G. and R. Rossi, 1987: The relationship between tropopause potential temperature and the buoyant energy of storm air. J. Atmos. Sci., **44**, 2902–2911.

Dopplick, T. G., 1972: Radiative heating of the global atmosphere. J. Atmos. Sci., **29**, 1278–1294.

Edmon Jr, H., B. Hoskins, and M. McIntyre, 1980: Eliassen-Palm cross sections for the troposphere. J. Atmos. Sci., **37**, 2600–2616.

Fierro, A. O., J. Simpson, M. A. LeMone, J. M. Straka, and B. F. Smull, 2009: On how hot towers fuel the Hadley cell: An observational and modeling study of line-organized convection in the equatorial trough from TOGA COARE. J. Atmos. Sci., **66**, 2730–2746.

Folkins, I., S. J. Oltmans, and A. M. Thompson, 2000: Tropical convective outflow and near surface equivalent potential temperatures. Geophys. Res. Lett., **27**, 2549–2552.

Fueglistaler, S., A. Dessler, T. Dunkerton, I. Folkins, Q. Fu, and P. W. Mote, 2009: Tropical tropopause layer. Rev. Geophys., **47**, RG1004.

Gettelman, A., P. M. d. F. Forster, M. Fujiwara, Q. Fu, H. Vömel, L. K. Gohar, C. Johanson, and M. Ammerman, 2004: Radiation balance of the tropical tropopause layer. J. Geophys. Res.: Atmos. (1984–2012), **109**, D07103.

Gill, A. E., 1982: Atmosphere-ocean dynamics, Vol. 30. Academic Press.

Grams, C. M., S. C. Jones, and C. A. Davis, 2013: The impact of Typhoon Jangmi (2008) on the midlatitude flow. Part II: Downstream evolution. Quart. J. Roy. Meteor. Soc., **139**, 2165–2180.

Grotjahn, R., 2003: Energy cycle. In Encyclopedia of atmospheric sciences, edited by James R Holton, Judith A Curry, and John A Pyle. Academic Press.

Hadley, G., 1735: Concerning the cause of the general trade-winds: By Geo. Hadley, Esq; FRS. Philosophical Transactions, **39**, 58–62.

Harr, P. A., D. Anwender, and S. C. Jones, 2008: Predictability associated with the downstream impacts of the extratropical transition of tropical cyclones: Methodology and a case study of Typhoon Nabi (2005). Mon. Wea. Rev., **136**, 3205–3225.

Hart, R. E., 2011: An inverse relationship between aggregate northern hemisphere tropical cyclone activity and subsequent winter climate. Geophys. Res. Lett., **38**, L01705.

Hartmann, D. L., 1994: Global physical climatology, Vol. 56. Academic Press.

Holland, G. J., 1983: Tropical cyclone motion: Environmental interaction plus a beta effect. J. Atmos. Sci., **40**, 328–342.

Holton, J., 2004: An introduction to dynamic meteorology. Elsevier Academic Press.

Hoskins, B. J., 1991: Towards a PV-θ view of the general circulation. Tellus A, **43**, 27–35.

Hummel, J. and W. Kuhn, 1981: Comparison of radiative-convective models with constant and pressure-dependent lapse rates. Tellus, **33**, 254–261.

Jin, Y., W. T. Thompson, S. Wang, and C.-S. Liou, 2007: A numerical study of the effect of dissipative heating on tropical cyclone intensity. Wea. Forecasting, **22**, 950–966.

Johnson, D. R., 1989: The forcing and maintenance of global monsoonal circulations: An isentropic analysis. Advances in Geophysics, **31**, 43–329.

Jones, S. C., et al., 2003: The extratropical transition of tropical cyclones: Forecast challenges, current understanding, and future directions. Wea. Forecasting, **18**, 1052–1092.

Kuo, F. S., Lue, H. Y., Fern, C. L., Röttger, J., Fukao, S., and Yamamoto, M, 2008: Studies of vertical fluxes of horizontal momentum in the lower atmosphere using the MU-radar. Ann. Geophys., **26**, 3765-3781.

Lang, A. A. and J. E. Martin, 2012: The structure and evolution of lower stratospheric frontal zones. Part 1: Examples in northwesterly and southwesterly flow. Quart. J. Roy. Meteor. Soc., **138**, 1350–1365.

Lang, A. A. and J. E. Martin, 2013: The structure and evolution of lower stratospheric frontal zones. Part II: The influence of tropospheric ascent on lower stratospheric frontal development. Quart. J. Roy. Meteor. Soc., **139**, 1798–1809.

Lilly, D. K., Nicholls, J. M., Kennedy, P. J., Klemp, J. B. and Chervin, R. M., 1982: Aircraft measurements of wave momentum flux over the Colorado Rocky Mountains. Quart. J. Roy. Meteor. Soc., **108**, 625–642.

Lorenz, E. N., 1955: Available potential energy and the maintenance of the general circulation. Tellus, **7**, 157–167.

Marshall, J. and R. A. Plumb, 2008: Atmosphere, ocean, and climate dynamics. Elsevier Academic Press.

Martin, J. E., 2006: Mid-latitude atmospheric dynamics: a first course. John Wiley & Sons.

Martin, J. E., 2014: Quasi-geostrophic diagnosis of the influence of vorticity advection on the development of upper level jet-front systems. Quart. J. Roy. Meteor. Soc., in press.

Michaud, R. and J. Derome, 1991: On the mean meridional transport of energy in the atmosphere and oceans as derived from six years of ECMWF analyses. Tellus A, **43**, 1–14.

Montgomery, M. T., M. E. Nicholls, T. A. Cram, A. B. Saunders, 2006: A Vortical Hot Tower Route to Tropical Cyclogenesis. J. Atmos. Sci., **63**, 355–386.

Namias, J. and P. F. Clapp, 1949: Confluence theory of the high tropospheric jet stream. J. Meteor. **6**, 330–336.

National Hurricane Center, 2001a: Tropical Depression Fifteen Discussion Number 5. [Available online at http://www.nhc.noaa.gov/archive/2001/dis/al152001.discus.005.html].

National Hurricane Center, 2001b: Tropical Storm Michelle Discussion Number 11. [Available online at http://www.nhc.noaa.gov/archive/2001/dis/al152001.discus.011.html].

National Hurricane Center, 2001c: Hurricane Michelle Discussion Number 27. [Available online at http://www.nhc.noaa.gov/archive/2001/dis/al152001.discus.027.html].

Newton, C. W. and E. Palmén, 1963: Kinematic and thermal properties of a large amplitude wave in the westerlies. Tellus, **15**, 99–119.

Ólafsson , H. and M. A. Shapiro, 2002: Observations and numerical simulations of a wake and corner winds in a strong windstorm over Iceland . *10th Conference on Mountain Meteorology,* 16–21 Jun. 2002, Park City, UT.

Orlanski, I. and J. P. Sheldon, 1995: Stages in the energetics of baroclinic systems. Tellus A, **47**, 605–628.

Petty, G. W., 2006: A first course in atmospheric radiation. Sundog Publishing.

Rauber, R., J. Walsh, and D. Charlevoix, 2012: Severe and hazardous weather: An introduction to high-impact meteorology. Kendall-Hunt Publishing.

Riemer, M. and S. C. Jones, 2010: The downstream impact of tropical cyclones on a developing baroclinic wave in idealized scenarios of extratropical transition. Quart. J. Roy. Meteor. Soc., **136**, 617–637.

Riemer, M., S. C. Jones, and C. A. Davis, 2008: The impact of extratropical transition on the downstream flow: An idealized modelling study with a straight jet. Quart. J. Roy. Meteor. Soc., **134**, 69–91.

Shapiro, M. A., L. Simon, H. Ólafsson, J. Doyle, P. K. Smolarkiewicz, 2002: Large-amplitude gravity-wave breaking over the Greenland lee and the subsequent formation of downstream synoptic-scale tropopause folding and stratospheric-tropospheric exchange. *10th Conference on Mountain Meteorology,* 16–21 Jun. 2002, Park City, UT.

Shapiro, M. A. and D. A. Keyser, 1990: Fronts, jet streams, and the tropopause. US Department of Commerce, National Oceanic and Atmospheric Administration, Environmental Research Laboratories, Wave Propagation Laboratory.

Sherwood, S. C., A. E. Dessler, 2003: Convective Mixing near the Tropical Tropopause: Insights from Seasonal Variations. J. Atmos. Sci., **60**, 2674–2685.

Sherwood, S. C., P. Minnis, and M. McGill, 2004: Deep convective cloud-top heights and their thermodynamic control during CRYSTAL-FACE. J. Geophys. Res.: Atmos. (1984–2012), **109**, D20119.

Shi, J.-J., S. Wei-Jen Chang, and S. Raman, 1990: A numerical study of the outflow layer of tropical cyclones. Mon. Wea. Rev., **118**, 2042–2055.

Simmons, A. J. and B. J. Hoskins, 1978: The life cycles of some nonlinear baroclinic waves. J. Atmos. Sci., **35**, 414–432.

Solomon, S., 2007: Climate change 2007-the physical science basis: Working group I contribution to the fourth assessment report of the IPCC, Vol. 4. Cambridge University Press.

Stohl, A., et al., 2003: Stratosphere-troposphere exchange: A review, and what we have learned from STACCATO. J. Geophys. Res.: Atmos. (1984–2012), **108**, 8516.

Straus, D. M. and J. Shukla, 2000: Distinguishing between the SST-forced variability and internal variability in mid latitudes: Analysis of observations and GCM simulations. Quart. J. Roy. Meteor. Soc., **126**, 2323–2350.

Thuburn, J. and G. C. Craig, 1997: GCM tests of theories for the height of the tropopause. J. Atmos. Sci., **54**, 869–882.

Trenberth, K. E. and D. P. Stepaniak, 2003: Seamless poleward atmospheric energy transports and implications for the Hadley circulation. J. Climate, **16**, 3706–3722.

Trenberth, Kevin E., 1986: An Assessment of the Impact of Transient Eddies on the Zonal Flow during a Blocking Episode Using Localized Eliassen-Palm Flux Diagnostics. J. Atmos. Sci., **43**, 2070–2087.

Tripoli, G. J., 2013: Upper level energy interactions between tropical cyclones and the environment. In 16th cyclone workshop.

Tripoli, G., C. Medaglia, S. Dietrich, A. Mugnai, G. Panegrossi, S. Pinori, and E. Smith, 2005: The 9-10 November 2001 Algerian flood: A numerical study. Bull. Amer. Meteor. Soc., **86**, 1229–1235.

Uccellini, L. W. and P. J. Kocin, 1987: The interaction of jet streak circulations during heavy snow events along the east coast of the United States. Wea. Forecasting, **2**, 289–308.

University of Wyoming, 2001a: 80035 SKRH Riohacha Observations at 12Z 31 Oct 2001. [Available online at http://weather.uwyo.edu/cgi-bin/sounding?region=naconf&TYPE= TEXT%3ALIST&YEAR=2001&MONTH=10&FROM=3100&TO=3112&STNM=80035.].

University of Wyoming, 2001b: 80001 SKSP San Andres Isl Observations at 12Z 31 Oct 2001. [Available online at http://weather.uwyo.edu/cgi-bin/sounding?region=naconf&TYPE=TEXT%3ALIST &YEAR=2001&MONTH=10&FROM=3100&TO=3112&STNM=80001.].

Widger Jr, W. K., 1949: A study of the flow of angular momentum in the atmosphere. J. Meteor. **6**, 292–299.

Yamazaki, Y. and W. Peltier, 2014: Spatiotemporal development of irreversible mixing in midlatitude baroclinic wave life cycles: Morphology, energetics, and nonisentropic mixing activity. J. Geophys. Res.: Atmos., **119**, 3663–3686.